

Constraints on the contributions to the observed binary black hole population from individual evolutionary pathways in isolated binary evolution

Simon Stevenson^{1,2}, and Teagan A. Clarke^{2,3}

¹ Centre for Astrophysics and Supercomputing, Swinburne University of Technology, John St, Hawthorn, Victoria- 3122, Australia

² The ARC Centre of Excellence for Gravitational Wave Discovery, OzGrav

³ School of Physics and Astronomy, Monash University, Clayton, Vic. 3800, Australia

Accepted 2022 October 10. Received 2022 October 9; in original form 2022 August 10

ABSTRACT

Gravitational waves from merging binary black holes can be used to shed light on poorly understood aspects of massive binary stellar evolution, such as the evolution of massive stars (including their mass-loss rates), the common envelope phase, and the rate at which massive stars form throughout the cosmic history of the Universe. In this paper we explore the *correlated* impact of these phases on predictions for the merger rate and chirp mass distribution of merging binary black holes, aiming to identify possible degeneracies between model parameters. In many of our models, a large fraction (more than 70% of detectable binary black holes) arise from the chemically homogeneous evolution scenario; these models tend to over-predict the binary black hole merger rate and produce systems which are on average too massive. Our preferred models favour enhanced mass-loss rates for helium rich Wolf–Rayet stars, in tension with recent theoretical and observational developments. We identify correlations between the impact of the mass-loss rates of Wolf–Rayet stars and the metallicity evolution of the Universe on the rates and properties of merging binary black holes. Based on the observed mass distribution, we argue that the $\sim 10\%$ of binary black holes with chirp masses greater than $40 M_{\odot}$ (the maximum predicted by our models) are unlikely to have formed through isolated binary evolution, implying a significant contribution ($> 10\%$) from other formation channels such as dense star clusters or active galactic nuclei. Our models will enable inference on the uncertain parameters governing binary evolution in the near future.

Key words: binary evolution – black hole – gravitational wave – supernova

1 INTRODUCTION

Almost 100 binary black hole mergers have now been observed by the LIGO (Aasi et al. 2015) and Virgo (Acernese et al. 2015) gravitational-wave observatories, as identified and published in a series of catalogues by the LIGO, Virgo and KAGRA Scientific Collaborations (Abbott et al. 2019; Abbott et al. 2021d,a,b). A number of additional candidates have been identified in analyses of the data by external groups (e.g., Nitz et al. 2021; Olsen et al. 2022).

Analyses of the compact binary population using phenomenological population models have allowed the merger rates, mass and spin distributions of binary black holes to be constrained (Abbott et al. 2021c). For example, Abbott et al. (2021c) find that the rate of binary black hole mergers at redshift $z = 0.2$ is $17\text{--}45 \text{ Gpc}^{-3} \text{ yr}^{-1}$, and increases with redshift, in agreement with the measured cosmic star formation history (Madau & Dickinson 2014). However, beyond identifying some large scale properties of the population, it is

difficult to relate these features to the underlying physics describing the formation of binary black holes.

The origin of these gravitational-wave sources is currently a major open question in astrophysics. Several potential formation scenarios have been proposed as being able to explain the rates and properties of the observed binary black hole mergers (for a recent high-level overview of binary black hole formation scenarios, see Mandel & Farmer 2022). These scenarios include the evolution of massive binary stars (Belczynski et al. 2016a; Stevenson et al. 2017a), and the dynamical formation of black hole binaries in star clusters (e.g., Rodriguez et al. 2016; Di Carlo et al. 2020b) or active galactic nuclei (e.g., Yang et al. 2020). These scenarios make different predictions for the properties of merging binary black holes, and predict a wide range of merger rates (Mandel & Broekgaarden 2022).

In this paper, we focus our attention on modelling the formation of binary black holes through isolated binary evolution (Belczynski et al. 2016a; Stevenson et al. 2017a). However, even within

this channel, there are a number of different possible evolutionary pathways which may contribute to the observed binary black hole population. The most well known scenario involves the evolution of initially wide binaries, that interact through phases of mass transfer and/or common envelope evolution that shrink the orbit of the binary, finally forming a binary black hole that can merge due to the emission of gravitational waves within the age of the Universe.

Another evolutionary pathway that has been explored recently is the formation of merging binary black holes through chemically homogeneous evolution (Mandel & de Mink 2016; Marchant et al. 2016; du Buisson et al. 2020; Riley et al. 2021). In this channel, stars born in binaries with very short orbital periods can become tidally locked, leading to them rotating rapidly, enhancing mixing within the star. This can lead to chemically homogeneous evolution (Maeder 1987), where essentially the entire star is converted to helium through nuclear burning. This avoids the phases of radial expansion experienced by more conventional stellar evolution pathways, and may potentially allow for the formation of massive binary black holes in low-metallicity environments. Each of these channels produces sub-populations of binary black holes with different characteristics (such as masses).

There are many uncertainties in the evolution of massive binary stars (e.g., Belczynski et al. 2022), such as which binaries enter and survive the common envelope phase (and what their final orbital properties are), what the final masses and kicks of compact objects formed in supernovae are, and what the mass loss rates of evolved, low metallicity massive stars are, among others. We discuss each of these phases of binary evolution in greater detail in Section 2.

The impact of these uncertainties on the predictions for binary black hole formation have been extensively studied in the literature, typically through the use of binary population synthesis models. Population synthesis codes commonly used to model gravitational-wave sources include STARTRACK (Belczynski et al. 2016a), MOBSE (Giacobbo et al. 2018) and COSMIC (Breivik et al. 2020). Many works have focused on varying a single parameter (corresponding to a single uncertain stage of binary evolution) at a time (e.g., Voss & Tauris 2003; Dominik et al. 2012; Kruckow et al. 2018). This strategy has been successful as it has a number of positive aspects. Restricting variations to one piece of physics at a time keeps the computational cost of these analyses under control. In addition, isolating the impact of a single piece of physics on binary evolution aids tremendously in interpreting the results of these controlled numerical experiments. The predictions from these population synthesis models can then be compared to gravitational-wave observations in order to place constraints on the underlying binary evolution processes (Stevenson et al. 2015).

For example, following the first observations of neutron star-black hole mergers (Abbott et al. 2021f), Broekgaarden & Berger (2021) compared the observed rates of binary neutron star, neutron star-black hole and binary black hole coalescences (Abbott et al. 2021c) to a suite of predictions from the set of population synthesis models from Broekgaarden et al. (2021); Broekgaarden et al. (2022a). They find that only models with low supernova kicks or high common envelope efficiencies match the observed compact binary merger rates. Similar conclusions were reached by Santoliquido et al. (2021).

However, this method of varying one parameter (or one assumption) at a time is clearly not sufficient to fully explore the model parameter space (see Figure 1). Any conclusions reached by comparing observations to a limited set of models may therefore be biased. This is because the combined impact of varying several different parameters simultaneously has not been explored, and two

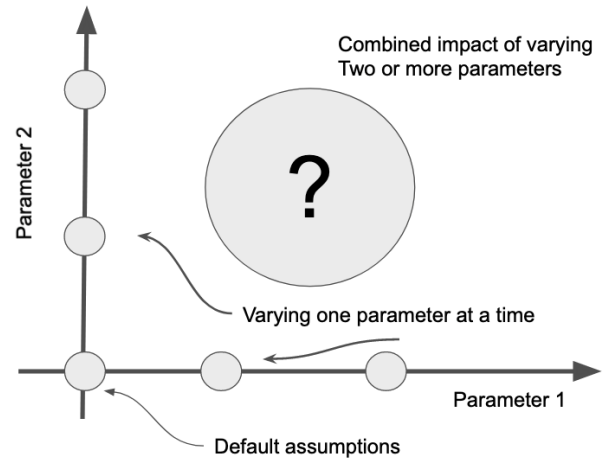


Figure 1. Cartoon illustrating the common method of exploring the binary evolution parameter space by varying a single parameter at a time. The gray circles represent the locations in the parameter space that models are computed. The large gray circle with a question mark highlights the parameter space unexplored with that method. Exploring this parameter space is the main aim of this work.

(or more) parameters may counteract one another, resulting in a *degeneracy* between multiple model parameters, such that the model results may be unchanged. Exploring these possibilities is the main aim of the present work.

Barrett et al. (2018) explored correlations between the impact of several binary evolution processes on the population of binary black holes predicted from isolated binary evolution. In particular, they used a Fisher matrix analysis to examine the correlations between the impact of the efficiency of the common envelope phase, supernova kicks and wind mass loss rates on the population of binary black holes. Barrett et al. (2018) explored how the predictions of their model varied under variations of four population parameters by a few percent around their values in a fiducial model using a method similar to that illustrated in Figure 1. They demonstrated that ~ 1000 gravitational-wave observations—a target expected to be reached in the next few years—would be sufficient to allow for precise measurements of many of these parameters. They found several interesting correlations, such as between the efficiency of common envelope evolution and the mass loss rates of Wolf–Rayet stars (see Section 2 for more details of the parameterisation of these phases). Whilst Barrett et al. (2018) demonstrated the viability of precisely constraining population parameters using gravitational-wave observations, and highlighted some interesting correlations between population parameters. However, the analysis of Barrett et al. (2018) was restricted to a small region of parameter space localised around a fiducial model, and thus does not give a clear picture of how the predictions of the model would vary across the broader parameter space. In addition, they assumed a single model for the cosmic star formation history of the universe, and did not account for the uncertainties there, which have since been shown to have an important impact on predictions for gravitational-wave mergers (e.g., Neijssel et al. 2019; Broekgaarden et al. 2022a). Finally, Barrett et al. (2018) did not self consistently include the chemically homogeneous evolution pathway for forming binary black holes in their modelling.

With respect to uncertainties in the cosmic star formation history, Broekgaarden et al. (2021); Broekgaarden et al. (2022a) took

a pioneering step by examining the impact of uncertainties in both the cosmic star formation rate history and massive binary evolution simultaneously (see also [Santoliquido et al. 2021](#)). However they still only varied one binary evolution parameter at a time (with one exception of one model).

In this paper we build upon these earlier works and examine the correlated impact of uncertainties in both massive binary stellar evolution and the cosmic star formation history on the properties of binary black hole mergers observable in gravitational waves. Understanding correlations in the space of models should ultimately aid in interpreting the constraints obtained on population synthesis models through comparison with observations (e.g., [Bouffanais et al. 2021a](#)).

The remainder of this paper is structured as follows: in Section 2 we describe the population synthesis code that we use to simulate populations of merging binary black holes, and give details of the parameterisations we employ for common envelope evolution, the mass-loss rates of Wolf–Rayet stars and the cosmic star formation history of the Universe, as well as of our model exploration. In Section 3 we summarise the currently observed sample of binary black hole mergers. We argue that the observed chirp mass distribution already appears to show evidence of contributions from multiple formation scenarios, as $\sim 10\%$ of binary black hole mergers are too massive to have formed through isolated binary evolution in our model, and must have formed through alternate channels such as in dense star clusters (e.g., [Rodríguez et al. 2018](#)) or active galactic nuclei (e.g., [Yang et al. 2019](#)). We describe the predictions of our large suite of 2,916 models in Section 4, focusing on demonstrating the range of binary black hole merger rates (Section 4.1) and mass distributions (Section 4.2) that are possible to attain through isolated binary evolution alone. We place particular emphasis on the contribution from binaries formed through chemically homogeneous evolution to the total population. We compare our models to current gravitational-wave observations in Section 4.3. We find that our preferred models have enhanced mass-loss rates for massive, evolved, helium-rich Wolf–Rayet stars. We also show that none of our models can produce a satisfactory match to the observed chirp mass distribution, and discuss some possible reasons for this discrepancy. Finally, we conclude and discuss limitations of the present work, and avenues for future work in Section 5.

2 METHOD

Most massive stars are known to be in binary or higher order multiple systems ([Sana et al. 2012](#); [Moe & Di Stefano 2017](#)). We model the evolution of massive isolated binaries using the rapid binary population synthesis suite COMPAS ([Stevenson et al. 2017a](#); [Vigna-Gómez et al. 2018](#); [Team COMPAS: Riley et al. 2022](#)).

The evolution of massive stars in COMPAS is approximated using the Single Stellar Evolution (SSE; [Hurley et al. 2000](#)) package, a set of analytic polynomial expressions fit to the set of detailed stellar models from [Pols et al. \(1998\)](#). The SSE package provides a fast and robust method to estimate parameters of stars such as their radii, luminosities and evolutionary timescales.

The implementation of binary evolution (e.g., mass transfer, common envelope evolution) in COMPAS broadly follows the prescriptions described in [Hurley et al. \(2002\)](#), with modifications as described in [Team COMPAS: Riley et al. \(2022\)](#). With the exception of the special case of chemically homogeneous evolution ([Riley et al. 2021](#)), tides are not currently implemented in COMPAS ([Team COMPAS: Riley et al. 2022](#)). We briefly summarise the

implementation of chemically homogeneous evolution in COMPAS in Section 2.1 below.

The initial parameters of our binaries are drawn from simple distributions, motivated by observations of massive binary stars. We draw the initial mass of the more massive star in the binary (the primary) from an initial mass function ([Kroupa 2001](#)) with a power-law slope of -2.3 for masses between $1 M_{\odot}$ and $150 M_{\odot}$. We draw the initial separations of the binaries from a log-uniform distribution between 0.01 and 1000 AU^1 . The mass ratio of the binary is then drawn from a uniform distribution ([Sana et al. 2012](#)), with the restriction that the mass of the secondary star must be greater than $0.1 M_{\odot}$. In order to reduce the initial parameter space, we assume that all massive binaries are initially circular; whilst this is not representative of the eccentricity distribution of massive binaries in nature, studies have shown that the impact on the results from binary population synthesis simulations is mild ([Hurley et al. 2002](#); [de Mink & Belczynski 2015](#)). We have also assumed that the distribution of initial binary properties is separable, which may not be the case ([Moe & Di Stefano 2017](#)), although studies have shown that properly accounting for this does not dramatically affect the predictions from population synthesis models ([Klencki et al. 2018](#)).

As discussed in the introduction, there are several different evolutionary pathways for binary black hole formation within the isolated binary evolution channel. Our COMPAS population synthesis models include the formation of merging binary black holes through stable mass transfer after the main sequence, common envelope evolution and chemically homogeneous evolution. However, it is worth noting that there may still be additional channels that contribute to the formation of binary black holes that are not currently modelled within COMPAS, such as formation through stable mass transfer on the main sequence (so called case A mass transfer) ([Valsecchi et al. 2010](#); [Qin et al. 2019](#); [Neijssel et al. 2021](#)), though we do not expect this to be the dominant channel (cf. [Gallegos-Garcia et al. 2022](#)).

We use the remnant prescription from [Fryer et al. \(2012\)](#) to determine the masses of black holes from the properties of a star (such as its total mass and core mass) at the time of core-collapse. In this model, most heavy black holes form through complete fallback with no associated kick. We assume that $0.1 M_{\odot}$ is lost through neutrinos in the collapse to a black hole ([Stevenson et al. 2019](#)).

Stellar evolution calculations make a robust prediction of a gap in the mass spectrum of black holes due to the effects of pair-instability supernovae ([Belczynski et al. 2016b](#); [Marchant et al. 2019](#); [Stevenson et al. 2019](#); [Farmer et al. 2019](#)). The exact location of this gap depends on the details of the stellar models, but typically models predict an absence of black holes in the mass range $50\text{--}120 M_{\odot}$ (e.g., [Woosley 2017](#)), whilst in some cases, stars that retain a massive hydrogen envelope may potentially produce black holes up to and beyond $70 M_{\odot}$ ([Costa et al. 2020](#); [Renzo et al. 2020](#); [Farrell et al. 2021](#)). Such stars are unlikely to exist in the compact binaries we consider here, as their hydrogen envelopes are likely removed through binary interactions. The effects of pair-instability supernovae are implemented in COMPAS as detailed in [Stevenson et al. \(2019\)](#), using a fit to the detailed models of [Marchant et al. \(2019\)](#). In our models, we find that the most massive black hole

¹ [Sana et al. \(2012\)](#) find a separation distribution which favours close binaries compared to our default separation distribution, which may be favourable for chemically homogeneous evolution. In this sense, our results for the fraction of binary black holes formed through chemically homogeneous evolution in Section 4 may be considered lower limits.

below the pair-instability mass gap has a mass of around $45 M_{\odot}$. We choose to focus our investigation on binary black holes where both black holes have masses below the mass gap for a number of reasons: 1) Only a few very massive stars ($> 150 M_{\odot}$) are known (e.g., [Figer 2005](#); [Crowther et al. 2010](#); [Bestenlehner et al. 2011](#)), their statistics are highly uncertain, and they may be the result of stellar mergers (e.g., [Banerjee et al. 2012](#)) 2) Stellar models for very massive stars are highly uncertain (e.g., [Agrawal et al. 2021](#)) 3) There are currently no robust observations of gravitational-wave sources from above the mass-gap ([Abbott et al. 2021b](#)).

As discussed above, our current understanding of several stages of massive binary evolution remain uncertain. In the following subsections we describe the prescriptions that we adopt for several of these phases, namely common envelope evolution, the mass-loss rates of massive stars, and the cosmic star formation history of the Universe. We give details of our default assumptions, as well as the variations that we consider.

2.1 Chemically homogeneous evolution

Massive close binaries may experience enhanced mixing due to tidal locking, leading to chemically homogeneous evolution. In this section we briefly summarise the implementation of chemically homogeneous evolution in COMPAS. For more details, see [Riley et al. \(2021\)](#).

The angular frequency of a tidally locked star is equal to the orbital frequency. It has previously been shown that there is a threshold angular frequency, beyond which stars experience chemically homogeneous evolution. In COMPAS, this threshold is determined by fits to one-dimensional rotating massive star models, calculated using Modules for Experiments in Stellar Astrophysics (MESA; [Paxton et al. 2011](#)), as described in [Riley et al. \(2021\)](#), as a function of mass and metallicity. If the angular frequency of a star on the zero-age main-sequence exceeds this threshold, it is assumed to evolve chemically homogeneously. We employ the variant of chemically homogeneous evolution within COMPAS that requires this threshold to be met throughout the main-sequence.

In COMPAS, we assume that the radius of a chemically homogeneously evolving star remains fixed to its zero-age main-sequence radius, whilst its luminosity is assumed to be the same as the luminosity of a normal, slowly rotating main-sequence star of the same fractional age ([Hurley et al. 2000](#)).

At the end of the main sequence, the star is assumed to evolve directly to the helium main-sequence (as given by [Hurley et al. 2000](#)), with the same mass as the total mass of the star at the end of the hydrogen main sequence.

2.2 Common envelope evolution

One of the most famous (and least understood) phases in the evolution of massive binaries is the common envelope phase ([Paczynski 1976](#); [Ivanova et al. 2013](#)), in which unstable mass transfer from an evolved giant star onto a compact star (such as a black hole) leads to the black hole orbiting inside of the envelope of the giant star. The black hole spirals in towards the core of the giant star due to drag forces, and in doing so injects energy into the envelope of the giant. If sufficient energy is available, the inspiral may be halted (after a dramatic reduction of the binary orbital separation) and the envelope may be ejected.

We make the standard assumption that some fraction α_{CE} of the orbital energy can be used to unbind the envelope ([Webbink](#)

1984; [de Kool 1990](#))

$$E_{\text{bind}} = \alpha_{\text{CE}} \Delta E_{\text{orb}}, \quad (1)$$

where the envelope binding energy is given by

$$E_{\text{bind}} = -\frac{GM M_{\text{env}}}{\lambda R}. \quad (2)$$

In this expression, M is the total mass of a star, whilst M_{env} is its envelope mass and R its radius. The envelope binding energy, E_{bind} , is parameterised by the dimensionless parameter λ . We use the fitting formulae for λ , constructed using a set of detailed stellar models, from [Xu & Li \(2010\)](#).

For the typical common envelope phase of interest en route to the formation of a binary black hole, ΔE_{orb} is given by

$$\Delta E_{\text{orb}} = -\frac{GM_{\text{BH,pre}} M_{\text{comp,pre}}}{2a_{\text{pre-CE}}} - \frac{GM_{\text{BH,post}} M_{\text{comp,post}}}{2a_{\text{post-CE}}}, \quad (3)$$

where $a_{\text{pre-CE}}$, $M_{\text{BH,pre}}$ and $M_{\text{comp,pre}}$ are the orbital separation, black hole mass and companion mass prior to the common envelope event, and $a_{\text{post-CE}}$, $M_{\text{BH,post}}$ and $M_{\text{comp,post}}$ are the same quantities afterwards. Larger values of α_{CE} represent a more efficient use of the orbital energy to unbind the envelope, resulting in wider post-common envelope binary separations. Our default model assumes $\alpha_{\text{CE}} = 1$ for all common envelope events (we discuss this potentially problematic assumption in Section 5).

If (as formulated here) the only available source of energy is the orbital energy then $0 \leq \alpha_{\text{CE}} \leq 1$. However, there may be additional energy sources available beyond the orbital energy, such as recombination energy ([Ivanova et al. 2015](#); [Ivanova 2018](#); [Kruckow et al. 2016](#); [Reichardt et al. 2020](#); [Lau et al. 2022](#)) or accretion-powered jets (e.g., [Soker et al. 2019](#); [Grichener & Soker 2021](#)), implying that $\alpha_{\text{CE}} > 1$ may be possible. Indeed, some observations of post-common envelope binaries (though these are typically of much lower mass than the systems of interest here) seem to suggest the need for additional energy sources (e.g., [De Marco et al. 2011](#); [Iaconi & De Marco 2019](#)). Recent simulations of the common envelope phase in massive binaries have found a range of effective values for α_{CE} ([Fragos et al. 2019](#); [Law-Smith et al. 2020](#); [Lau et al. 2022](#); [Moreno et al. 2021](#)). We therefore explore the range $0.1 \leq \alpha_{\text{CE}} \leq 10$. Since we are uncertain a priori whether $\alpha_{\text{CE}} > 1$ or $\alpha_{\text{CE}} < 1$, we explore both regimes with a similar number of models.

In addition to the uncertainty of the α_{CE} parameter (or equivalently, the mapping between initial conditions and final outcomes of the common envelope phase), there are several other uncertainties associated with common envelope evolution that we do not consider in detail here. Firstly, estimates of envelope binding energies from detailed stellar models are sensitive to assumptions made in those models, such as the boundary between the core and the envelope of the star ([Tauris & Dewi 2001](#); [Kruckow et al. 2016](#)). Since the product of α_{CE} and λ is relevant in determining the outcome of common envelope evolution, our models with different values of α_{CE} could also be viewed as probing systematic over/underestimations of the envelope binding energies. Secondly, modern detailed stellar models of massive stars seem to indicate that ejection of the envelopes of massive, low metallicity stars may only be possible for supergiants in a narrow range of orbital periods ([Klencki et al. 2021](#); [Marchant et al. 2021](#)).

An additional uncertainty in common envelope evolution regards the fate of donor stars crossing the Hertzsprung gap. Stars just beyond the main sequence may not have developed sufficient core-envelope separation to be able to survive the common envelope

phase. Here we assume that all common envelope events involving a donor star on the Hertzsprung gap result in stellar mergers, following [Belczynski et al. \(2007\)](#) and [Dominik et al. \(2012\)](#).

Since binary black holes formed through the chemically homogeneous evolution pathway do not experience the common envelope phase, we do not expect our treatment of this phase to affect our predictions for this scenario.

2.3 Massive star winds

Massive stars can lose substantial amounts of mass throughout their lives through strong stellar winds (see [Vink 2021](#), for a review). There are several stages of massive stellar evolution where mass loss can be important, including line-driven winds from hot OB stars on the main sequence ([Vink et al. 2001](#)), dust driven winds from cool red supergiants ([Mauron & Josselin 2011](#); [Beasor et al. 2020](#)), and eruptive mass loss from luminous blue variables ([Vink & de Koter 2002](#); [Smith 2017](#))². The amount of mass a star loses throughout its life can impact the evolution of massive stars and the final properties of their remnants ([Renzo et al. 2017](#)).

Mass loss rates for stars at each of these different evolutionary stages can be estimated either from observations, or from theory. For massive, low metallicity stars (the same stars expected to produce many of the observed binary black holes), the mass loss rates are poorly constrained from observation, as massive stars are inherently rare and short lived, and there are only a few local low metallicity environments (such as the Magellanic clouds) where low metallicity stars can be studied in detail.

We follow the default mass loss prescription in COMPAS ([Team COMPAS: Riley et al. 2022](#)) (see also [Belczynski et al. 2010](#)). We give more details about the mass loss rates assumed for Wolf–Rayet stars in the section below.

2.3.1 Wolf–Rayet stars

Wolf–Rayet stars³ are massive, evolved, helium rich stars with high mass loss rates of $> 10^{-5} M_{\odot} \text{ yr}^{-1}$ (e.g., [Barlow et al. 1981](#)). They may be formed in single stellar evolution by the removal of the hydrogen envelope of a star through stellar winds, or, perhaps more commonly, can be formed in binary evolution when the hydrogen envelope is removed through mass transfer ([Paczynski 1967](#)).

Mass loss during the Wolf–Rayet stage is important for determining the masses of black holes ([Belczynski et al. 2010](#); [Higgins et al. 2021](#); [Vink et al. 2021](#)). It is particularly important for binary black holes formed through the chemically homogeneous evolution channel ([Mandel & de Mink 2016](#); [Riley et al. 2021](#)). Firstly, mass loss may lead to a widening of the binary orbit, resulting in binaries no longer being in close enough orbits to maintain high rotation rates, and secondly that mass loss carries away angular momentum, which again may slow the rotation of stars, reducing the parameter space for chemically homogeneous evolution.

Following [Belczynski et al. \(2010\)](#) we assume that the mass loss rates of Wolf–Rayet stars are given by

$$\dot{M}_{\text{WR}} = f_{\text{WR}} \times 10^{-13} \left(\frac{L}{L_{\odot}} \right)^{1.5} \left(\frac{Z}{Z_{\odot}} \right)^m M_{\odot} \text{ yr}^{-1}, \quad (4)$$

² Stars evolving chemically homogeneously do not experience the red supergiant or luminous blue variable phases, and thus are not impacted by mass loss during these phases

³ We do not distinguish between the various subclasses of Wolf–Rayet stars (e.g., WN, WC, WO).

where L is the stellar luminosity, Z is the metallicity and f_{WR} is a scaling parameter introduced to allow us to easily vary the mass loss rates during this phase of stellar evolution ([Barrett et al. 2018](#); [Team COMPAS: Riley et al. 2022](#)). This prescription is derived from the results of theoretical models. The dependence of the mass loss rate with luminosity comes from [Hamann & Koesterke \(1998\)](#), while the parameter $m = 0.86$ determines the scaling of the mass loss rates with metallicity, and is determined from theoretical models by [Vink & de Koter \(2005\)](#). Our default choice is $f_{\text{WR}} = 1$.

Recently, several authors have suggested that Equation 4 may either under- or over-estimate the mass loss rates of Wolf–Rayet stars (see e.g., discussion in [Sander & Vink 2020](#), in particular their Figure 1).

On the theoretical side, [Vink \(2017\)](#) presented a new set of mass-loss rates for stripped stars that are significantly lower than those found by [Hamann & Koesterke \(1998\)](#). Building on the work of [Vink \(2017\)](#), [Sander & Vink \(2020\)](#) found that helium star mass loss rates may decrease dramatically below a transition luminosity.

On the empirical side, a popular formula for Wolf–Rayet star mass loss, utilised in many stellar evolution codes, was devised by [Nugis & Lamers \(2000\)](#). This expression predicts higher mass loss rates than those from [Hamann & Koesterke \(1998\)](#) or [Vink \(2017\)](#). Recently, [Tramper et al. \(2016\)](#) found even higher mass loss rates than those found by [Nugis & Lamers \(2000\)](#). [Hamann et al. \(2019\)](#) utilised improved constraints on the distances to Galactic WN stars from *Gaia* to update their measurements of the mass loss rates. They found a large scatter in the mass loss rates as a function of luminosity, with a weaker dependence on luminosity than found by [Nugis & Lamers \(2000\)](#). [Yoon \(2017\)](#) found that a mild increase in the mass-loss rates of Wolf–Rayet stars by about 60% (i.e., $f_{\text{WR}} \sim 1.6$) compared to commonly used mass-loss prescriptions improved the agreement between their stellar models and observations of faint WC/WO stars. [Neijssel et al. \(2021\)](#) argue for reduced wind mass loss rates for helium stars (compared to Equation 4) in order to explain the high black hole mass inferred in the Galactic X-ray binary Cygnus X-1 ([Miller-Jones et al. 2021](#)).

We compare the mass-loss rates predicted by these prescriptions as a function of stellar luminosity at solar metallicity ($Z = Z_{\odot}$) in Figure 2. We find that varying f_{WR} in the range 0.1–10 sufficiently captures the range of predictions from these models. Similarly to the case of the common envelope efficiency parameter α_{CE} , we choose to design our grid of simulations such that we have an equal number of models with $f_{\text{WR}} > 1$ and $f_{\text{WR}} < 1$.

2.4 Cosmic star formation history

Even though massive stars live for only a few million years, merging compact neutron star and black hole binaries can have long delay times of up to billions of years (Gyr) between the formation of the binary and the eventual gravitational-wave driven merger ([Neijssel et al. 2019](#); [Broekgaarden et al. 2021](#)). This means that compact binaries that merge in the local universe and are observable by LIGO/Virgo may be the products of stars formed at (much) higher redshifts (e.g., [Belczynski et al. 2016a](#); [Neijssel et al. 2019](#)).

The overall star formation rate density budget of the universe is reasonably well constrained at redshifts $z \lesssim 2$, where the star formation rate is observed to increase by a factor of ~ 10 between the local universe ($z = 0$) and the peak of star formation around redshift $z = 2$. At higher redshifts, the total star formation rate is more poorly constrained observationally, largely due to the impact of dust extinction ([Madau & Dickinson 2014](#); [Finkelstein 2016](#)).

One can incorporate the star formation history in a number

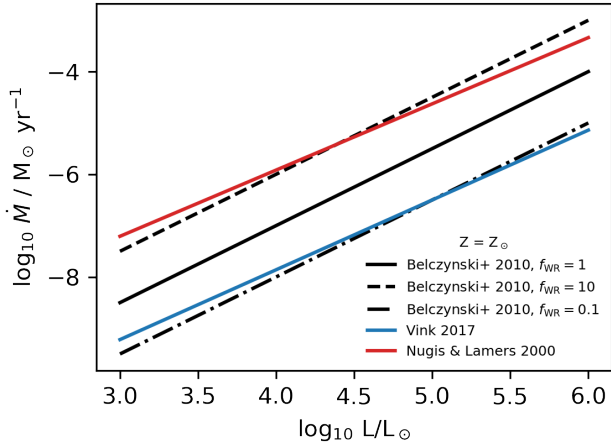


Figure 2. Mass loss rates for WR stars as a function of stellar luminosity at solar metallicity ($Z = Z_{\odot}$), as predicted by the prescriptions discussed in Section 2.3.1. The solid black line denotes our standard assumption for WR mass loss rates ($f_{\text{WR}} = 1$) (Hamann & Koesterke 1998; Belczynski et al. 2010). The dashed black line shows the same prescription, but with $f_{\text{WR}} = 10$, whilst the dot-dashed black line shows the values for $f_{\text{WR}} = 0.1$. The solid blue line shows the predictions from Vink (2017), whilst the solid red line shows the predictions from Nugis & Lamers (2000).

of ways. A common method is to make use of analytic or phenomenological models for the cosmic star formation rate density as a function of redshift, calibrated to observations (Madau & Dickinson 2014). Alternatively, one can attempt to use predictions of the star formation rate at high redshift from cosmological simulations. Several groups have pursued this approach, combining the outputs of various combinations of population synthesis models and cosmological simulations to study the population of gravitational-wave mergers (e.g., Mapelli et al. 2017; O’Shaughnessy et al. 2017; Lamberts et al. 2018; Mapelli & Giacobbo 2018; van Son et al. 2022b; Briel et al. 2022).

In this paper, we opt to use simple phenomenological model of the cosmic star formation rate, which can then be calibrated to match observations. In particular, we use the following description of the cosmic star formation rate density following Madau & Dickinson (2014)

$$\psi(z) = \frac{d^2 M_{\text{SFR}}}{dt_s dV_c}(z) = a \frac{(1+z)^b}{1 + [(1+z)/c]^d} M_{\odot} \text{yr}^{-1} \text{Mpc}^{-3}, \quad (5)$$

where a , b , c and d are fitting parameters. Madau & Dickinson (2014) find that $a = 0.015$, $b = 2.7$, $c = 2.9$ and $d = 5.6$. Madau & Fragos (2017) updated this fit and found $a = 0.01$, $b = 2.6$, $c = 3.2$ and $d = 6.2$. Neijssel et al. (2019) calibrated the parameters for Equation 5 by comparing COMPAS models to the rate and mass distribution of binary black holes observed during the first and second observing runs of Advanced LIGO (Abbott et al. 2019). They found $a = 0.01$, $b = 2.77$, $c = 2.9$ and $d = 4.7$. We note however that at that time, COMPAS did not include the chemically homogeneous evolution channel. Since the inclusion of this formation channel changes the predicted binary black hole mass distribution and rate (Riley et al. 2021), we expect that the best fit parameters for Equation 5 will change. At high redshift, the total star formation rate remains highly uncertain, primarily due to the impact of dust extinction. Strolger et al. (2004) found a star formation rate which

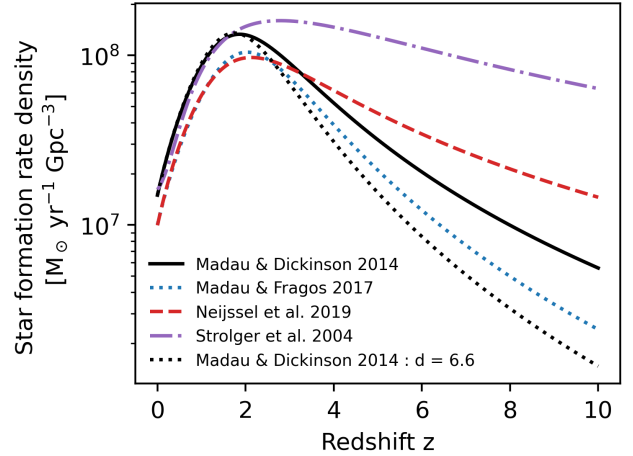


Figure 3. Star formation rate density as a function of redshift. The solid black line shows the model from Madau & Dickinson (2014); the dashed black lines uses their default values for a , b and c (see Equation 5), whilst using either $d = 3.6$ (upper curve) or $d = 6.6$ (lower curve), indicating the range of our prior on d (see Table 1). We also show the fit using the parameters from Madau & Fragos (2017) as the dotted blue curve. The dot-dashed purple curve uses the star formation rate model 1 from Strolger et al. (2004). The dashed red curve shows the phenomenological model from Neijssel et al. (2019).

remains much higher than that given by Madau & Dickinson (2014) at high redshift ($z > 2$). A similar result was found recently by Enia et al. (2022) who studied galaxies using radio observations.

As can be seen from Equation 5, when formulated this way, the SFR has 4 free parameters. To limit the parameter space we only consider variations in d , which we consider to be the most uncertain parameter, as it controls the star formation rate at high redshift in this model, which is where the star formation rate is most uncertain. Based on the literature discussed above, we find that varying d between 3.5 and 7.0 covers the range of high-redshift star formation rates discussed by the authors above. We show a range of prescriptions for the star formations rate as a function of redshift in Figure 3.

2.4.1 Metallicity specific star formation history

In addition to the total star formation rate at a given redshift, the distribution of star forming mass with gas phase metallicity is also a crucially important ingredient in the formation of compact object binaries (and binary black holes in particular) since both the evolution of massive stars and the formation of black holes are sensitive to the stellar metallicity (as discussed in Section 2.3).

We refer to this quantity as the metallicity-specific star formation rate, given by

$$\Phi(Z, z) = \psi(z) \frac{dN}{dZ}, \quad (6)$$

where ψ is the total star formation rate given by Equation 5 and dN/dZ is the distribution of metallicities.

In COMPAS we make use of a phenomenological gas-phase metallicity distribution, which is modelled as a log-normal distribution with a mean metallicity $\langle Z \rangle$, with a standard deviation σ_Z (Neijssel et al. 2019; Team COMPAS: Riley et al. 2022), independent of redshift. Our default model assumes that $\sigma_Z = 0.5$ (Neijssel

et al. 2019). In our model, the mean metallicity $\langle Z \rangle$ scales with redshift z as

$$\langle Z \rangle = \mu_0 \times 10^{m_z z}, \quad (7)$$

or equivalently

$$\log_{10} \langle Z/Z_\odot \rangle = \log_{10} \left(\frac{\mu_0}{Z_\odot} \right) + m_z z, \quad (8)$$

where μ_0 is the mean metallicity at redshift $z = 0$, Z_\odot is the solar metallicity and m_z describes the scaling with redshift, following Langer & Norman (2006). Langer & Norman (2006) assumed that $\mu_0 = Z_\odot$ and $m_z = 0.15$, based upon observationally determined metallicities for star forming galaxies at $z < 1$ (Kewley & Kobulnicky 2005). A more recent study expanding the sample of galaxies (and the range of redshifts) by Yuan et al. (2013) finds overall similar results.

Based on observations, Madau & Fragos (2017) assume that the mean metallicity as a function of redshift is given by $\log \langle Z/Z_\odot \rangle = 0.153 - 0.074z^{1.34}$. There is no set of parameters for Equation 7 that would exactly reproduce the fit from Madau & Fragos (2017). Madau & Fragos (2017) find that $\log_{10} \langle Z_0/Z_\odot \rangle = 0.153$, implying that the average star formation in the local universe is super-solar.

Neijssel et al. (2019) found that $\mu_0 = 0.035$ and $m_z = -0.23$, combined with the default binary evolution parameters in COMPAS, gave a good agreement with the observed binary black hole mass distribution and rate. As mentioned above, this did not include the contribution of the chemically homogeneous evolution channel and thus the best fit parameters for Equation 7 may also change. We show the evolution of the mean metallicity with redshift, as determined by these three prescriptions, in Figure 4. We use the variation between these prescriptions to motivate the range of values of Z_0 that we explore. We find a range of Z_0 between 0.01 and 0.05 captures the uncertainty in the average metallicity of star forming gas at redshift 0 (Table 1).

The evolution of the metallicity specific star formation rate with redshift is highly uncertain (Chruslinska et al. 2019; Chruslinska & Nelemans 2019), and uncertainties in this quantity translate to large uncertainties in predictions for the rates and properties of binary black hole mergers (Neijssel et al. 2019; Belczynski et al. 2020; Tang et al. 2020; Boco et al. 2021; Santoliquido et al. 2021; Broekgaarden et al. 2022a).

In addition to the uncertainties related to the average star formation rate at redshift 0, there are also uncertainties related to the evolution of the average metallicity with redshift (as characterised by m_z) and the distribution of metallicities at a given redshift, as characterised by σ_Z , which may or may not be redshift-dependent. We leave a more thorough exploration of this problem for future work.

2.5 Merger rates

One of the key observables predicted by our binary population synthesis models is the rate of binary black hole mergers. In this section we define several different rates that we quote in this work.

We calculate the differential merger rate of binary black holes at redshift z per unit volume per unit time as a function of chirp mass \mathcal{M} according to

$$\frac{dN}{dV_c dt_s d\mathcal{M}}(z) = \int dZ \int d\tau_{\text{delay}} \mathcal{R}_{\text{form}} \Phi(Z, t_{\text{form}}), \quad (9)$$

where t_s is the time measured in the source frame of the merging binary black hole, and V_c is the comoving volume. The term

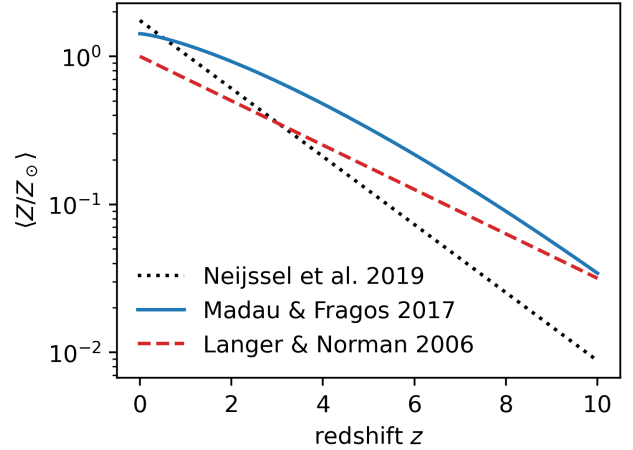


Figure 4. Mean metallicity of gas-phase star forming material as a function of redshift as determined by the models discussed in Section 2.4.1. The solid blue line shows the mean metallicity as given by the fit from Madau & Fragos (2017). The dashed red line corresponds to Equation 7 with values taken from Langer & Norman (2006), whilst the dotted black line uses values from Neijssel et al. (2019).

$\Phi(Z, t_{\text{form}})$ in Equation 9 is the metallicity-specific star formation rate, given by Equation 6.

The binary chirp mass \mathcal{M} is a combination of the component masses m_1 and m_2 given by

$$\mathcal{M} = \frac{(m_1 m_2)^{3/5}}{(m_1 + m_2)^{1/5}}. \quad (10)$$

The term $\mathcal{R}_{\text{form}}$ in Equation 9 describes the formation rate of binary black holes estimated by COMPAS, and is given by

$$\mathcal{R}_{\text{form}} = \frac{dN}{dM_{\text{form}} d\tau_{\text{delay}} d\mathcal{M}}, \quad (11)$$

where M_{form} is the amount of star forming mass and τ_{delay} is the delay time between star formation and the compact object merger (Peters 1964). The time at which the progenitor stars form is related to the time the binary merges t_{merge} by $t_{\text{form}} = t_{\text{merge}}(z) - \tau_{\text{delay}}$ (e.g., Barrett et al. 2018).

Where necessary, we adopt the cosmological parameters for a flat Λ -CDM universe from Hinshaw et al. (2013) as implemented in ASTROPY (Astropy Collaboration et al. 2013, 2018, 2022).

The merger rate at redshift z is then given by integrating Equation 9 over all chirp masses

$$\mathcal{R}(z) = \frac{dN}{dV_c dt_s} = \int \frac{dN}{dV_c dt_s d\mathcal{M}}(z) d\mathcal{M}. \quad (12)$$

We define the local merger rate as the value given by Equation 12 evaluated at redshift $z = 0$.

The predicted observed chirp mass distribution differs from that given by Equation 9 and is given by

$$\frac{dN_{\text{det}}}{dt_{\text{obs}} d\mathcal{M}} = \int dz \frac{dN}{dt_s dV_c d\mathcal{M}} \frac{dV_c}{dz} \frac{dt_s}{dt_{\text{obs}}} P_{\text{det}}, \quad (13)$$

where the first term inside the integral is given by Equation 9, $dt_{\text{obs}} = (1+z)dt_s$ is the time measured in the frame of the observer,

dV_c/dz is the volume element⁴ and P_{det} is the detection probability for a given binary (Barrett et al. 2018).

The detection probability P_{det} for a given binary depends on the parameters of that binary, such as its masses, spins and distance, and therefore describes the selection effects imposed by gravitational-wave observatories. We determine P_{det} using the method described by Barrett et al. (2018). In summary, we use a phenomenological model (IMRPHENOMPv2; Khan et al. 2016) that includes the inspiral, merger and ringdown phases of the gravitational waveform. When calculating sensitivities, we neglect black hole spins which are expected to play a subdominant role in the detectability of binary black holes (Ng et al. 2018). Regardless, the majority of black hole spins inferred from gravitational-wave observations appear to be small (Farr et al. 2017; Abbott et al. 2021e; Galaudage et al. 2021). Using this model, we estimate the signal-to-noise ratio a given binary would produce in a single gravitational-wave observatory operating with a sensitivity comparable to that of the LIGO interferometers during their third observing run (O3; Abbott et al. 2021b; Abbott et al. 2020a). Following convention, we assume that binaries that produce a signal-to-noise ratio greater than 8 are detected.

The predicted detection rate is given by integrating Equation 13 over all chirp masses

$$\mathcal{R}_{\text{det}} = \frac{dN_{\text{det}}}{dt_{\text{obs}}} = \int dM \frac{dN}{dt_{\text{obs}} dM}, \quad (14)$$

and the expected number of detections in an observing period of duration T_{obs} is given by

$$N_{\text{det}} = \mathcal{R}_{\text{det}} T_{\text{obs}}. \quad (15)$$

2.6 Model exploration

As discussed in the introduction, there are many uncertainties in massive binary evolution, and ideally, population synthesis analyses would explore the full range of possibilities for each uncertainty. However, if one wishes to explore N_{hyper} hyperparameters with N_{explore} models per hyperparameter, then the total number of models required will be roughly $N_{\text{explore}}^{N_{\text{hyper}}}$. This number can very quickly become large for even moderate values of N_{explore} and N_{hyper} . This is the well known *curse of dimensionality*.

In order to avoid the *curse of dimensionality* we have chosen to limit the parameters we explore to the 4 parameters introduced earlier in Section 2, namely the efficiency of common envelope evolution (α_{CE}), the mass-loss rates of Wolf–Rayet stars (f_{WR}), the cosmic star formation rate at high redshift (d) and the average metallicity of star formation at redshift 0 (Z_0), which we term *population hyperparameters* (Barrett et al. 2018). We have chosen these parameters as previous work has shown that they have the largest impact on predictions for merging binary black holes (e.g., Riley et al. 2021; Broekgaarden et al. 2022a)

We construct our grid of models using Latin hypercube sampling (McKay et al. 1979) as implemented in the Python package PYDOE. We use an algorithm that maximises the minimum distance between points (Morris & Mitchell 1995). This distribution has the property that the marginalised one-dimensional distributions are uniform in the sampled parameter. We draw 50 samples using the Latin hypercube sampling, and additionally include the edges of the

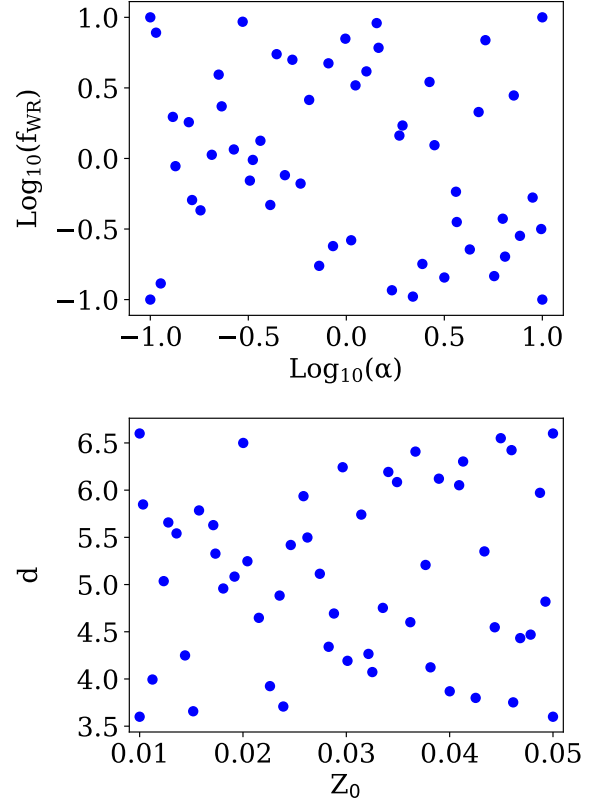


Figure 5. Hyperparameters at which we calculate our population synthesis models, drawn using Latin hypercube sampling. The top panel shows the binary evolution parameters α and f_{WR} , whilst the bottom panel shows the parameters governing the cosmic star formation history, d and Z_0 .

parameter space. In total we sample $N = 54$ models with different combinations of the binary evolution parameters α_{CE} and f_{WR} .

Since they are decoupled from the underlying binary evolution, we explore the impact of uncertainties in the cosmic star formation history in post-processing. We use $N = 54$ combinations of SFR parameters for each combination of binary evolution parameters. Thus in total we explore $54 \times 54 = 2,916$ different models. We list the ranges of parameters we explore in Table 1. We draw α_{CE} by sampling $\log_{10}(\alpha_{\text{CE}})$ between $\log_{10}(\alpha_{\text{CE}}^{\text{min}})$ and $\log_{10}(\alpha_{\text{CE}}^{\text{max}})$, as specified in Table 1. Similarly, for the mass-loss rates of Wolf–Rayet stars, we determine the multiplier f_{WR} by drawing $\log_{10}(f_{\text{WR}})$ between $\log_{10}(f_{\text{WR}}^{\text{min}})$ and $\log_{10}(f_{\text{WR}}^{\text{max}})$. We draw the values of d and Z_0 between d^{min} and d^{max} , and Z_0^{min} and Z_0^{max} respectively. We show these samples in Figure 5.

For each model, we sample the metallicities of the binaries uniformly in the log between $Z_{\text{min}} = 10^{-4}$ and $Z_{\text{max}} = 0.03$ (Team COMPAS; Riley et al. 2022). This helps to mitigate issues associated with using grids of discrete metallicities, such as sharp features (‘spikes’) in the mass distribution of binary black holes (Dominik et al. 2015). We draw $N = 10^6$ binaries from each model.

Our models typically take ~ 12 hrs to compute on a single node on the OzSTAR supercomputer at Swinburne University of Technology. We make use of the trivial parallelisability of COMPAS in order to run multiple models in parallel, utilising up to 54 cores. We find that post-processing contributes only a negligible additional

⁴ We calculate the cosmological volume element dV_c/dz using ASTROPY (Astropy Collaboration et al. 2013, 2018, 2022)

Parameter	Fiducial value	Minimum	Maximum
Common envelope efficiency (α_{CE})	1	0.1	10
Wolf-Rayet mass-loss rate (f_{WR})	1	0.1	10
High-redshift star-formation rate (d)	4.7	3.6	6.6
Average star-formation metallicity (Z_0)	0.035	0.01	0.05

Table 1. Hyperparameters explored in this paper. The fiducial value refers to our default assumption for each parameter, taken from [Team COMPAS: Riley et al. \(2022\)](#). We also list the minimum and maximum value that each parameter is varied between (as justified in Section 2).

computational cost. More sophisticated sampling techniques could reduce the computational cost of exploring the parameter space of binary evolution, or equivalently, either allow one to broaden the parameter space explored, or decrease statistical uncertainties at a fixed computational cost ([Broekgaard et al. 2019](#)).

3 OBSERVATIONAL SAMPLE

Before comparing our models to the gravitational-wave observations, we first discuss the details of our sample selection. We start from all gravitational-wave events included in the catalogue of gravitational-wave transients published following LIGO and Virgo’s third observing run (GWTC-3; [Abbott et al. 2021b](#)). This includes all events that have an estimated probability of astrophysical origin, P_{astro} , greater than 0.5 ([Abbott et al. 2021b](#)). We begin by excluding all events in which the secondary has a mass m_2 consistent with a neutron star, since these could either be binary neutron star (such as GW170817 and GW190425; [Abbott et al. 2017, 2020c](#)) or neutron star-black hole (such as GW200105; [Abbott et al. 2021f](#)) binaries. We also choose to exclude the highly asymmetric binary GW190814 ([Abbott et al. 2020d](#)), partly due to the uncertain classification of the secondary (which may either be the most massive neutron star or lightest black hole observed), and partly due to the mass ratio, which is difficult to produce through isolated binary evolution (though see [Zevin et al. 2020; Mandel et al. 2020; Antoniadis et al. 2022](#), for possible explanations in this context). We assume that the remainder of the population (79 events) are binary black holes.

As discussed in Section 2, binary evolution models (including COMPAS) predict the existence of a gap in the mass spectrum of black holes, beginning above $\sim 45 M_{\odot}$ (e.g., [Stevenson et al. 2019](#)), although uncertainties (mainly in nuclear reaction rates) may allow this value to be higher ([Farmer et al. 2019](#)). We find that the maximum binary black hole chirp mass does not vary significantly between our models. We find a maximum chirp mass of around $40 M_{\odot}$ in our models (see Section 4.2). We therefore choose to exclude all observed binary black holes with chirp masses greater than this value, as in our analysis, these events must be produced via other formation pathways such as hierarchical mergers of lower mass black holes through stellar dynamics (e.g., [Rodríguez et al. 2018; Yang et al. 2019; Di Carlo et al. 2020a; Mapelli et al. 2021a,b](#)). This excludes events such as GW190521 ([Abbott et al. 2020b,e](#)) and GW200220_061928 ([Abbott et al. 2021b](#)). Applying these selection criteria leaves us with a sample of 71 binary black hole observations. We plot the empirical cumulative distribution for the chirp masses of all observed binary black holes in the top panel of Figure 6, whilst we show only those events with a median chirp mass of less than $40 M_{\odot}$ in the middle panel of Figure 6. We show the fraction of binary black holes with a chirp mass greater than $40 M_{\odot}$ in Figure 7.

Intriguingly, we find that around 10% of binary black holes are excluded from our comparison as they have masses greater than that predicted in our models (Figure 7). This immediately implies that at

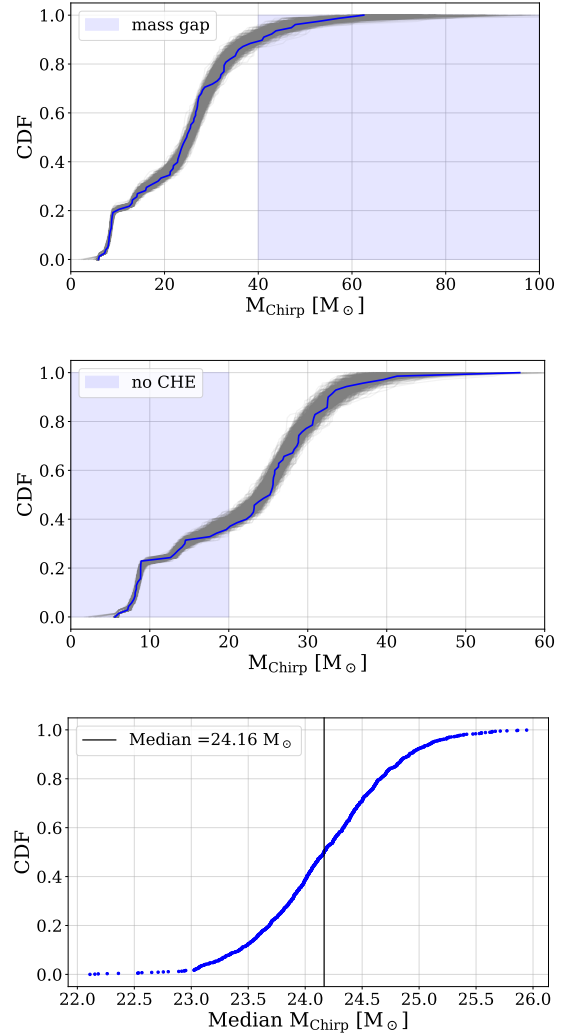


Figure 6. Empirical cumulative chirp mass distribution of binary black holes detected during the first three observing runs of Advanced LIGO and Virgo ([Abbott et al. 2019; Abbott et al. 2021d,b](#)). In the top panel, each of the 1000 lines is constructed by randomly drawing one sample from the posterior distribution for the chirp mass for each of the 79 binary black hole events observed in gravitational waves. The 10% of binary black holes with chirp masses greater than $40 M_{\odot}$ (shaded blue region) are unlikely to have formed through isolated binary evolution (see Section 3 for more discussion). In the middle panel we exclude all binary black holes with a median chirp mass greater than $40 M_{\odot}$. The solid blue lines in the top two panels highlight a single random cumulative distribution to guide the eye. The shaded blue region shows that of the binary black holes that can be formed through binary evolution, $\sim 40\%$ have masses less than the lowest mass produced through chemically homogeneous evolution. The bottom panel shows the cumulative distribution for the median observed chirp mass, which is around $25 M_{\odot}$.

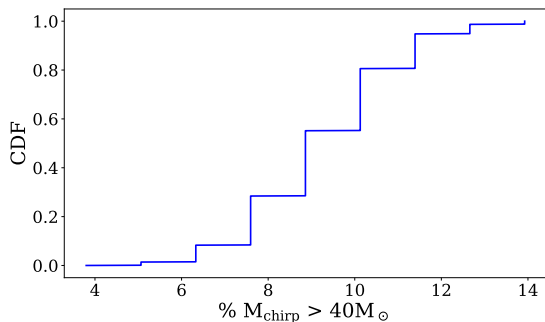


Figure 7. Cumulative distribution of the percentage of observed binary black holes with chirp masses greater than $40 M_{\odot}$, the maximum obtained in COMPAS (Stevenson et al. 2019). The histogram is generated from 1000 posterior samples for each of the 79 BBH events in GWTC-3 (Abbott et al. 2021b). Approximately nine percent of the observed BBH population have a chirp mass that cannot be reproduced in COMPAS.

least 10% of the observed binary black hole population is not formed through isolated binary evolution; we treat this fraction as a lower limit, since if there are contributions from other channels above a chirp mass of $40 M_{\odot}$, it is likely that there are contributions/events below this chirp mass limit too.

Some authors have come to similar conclusions based on alternate methods and lines of reasoning. By searching for signatures of eccentricity in the observed gravitational waveforms, Romero-Shaw et al. (2021, 2022) argue that up to 100% of binary black holes could be dynamically formed based on the observation of significant eccentricity in 4 binaries at the time of merger (which is not expected through isolated binary evolution), including the massive binary black hole merger GW190521 (Romero-Shaw et al. 2020; Bustillo et al. 2021; Gayathri et al. 2022). Using a combination of population synthesis models, Zevin et al. (2021) find that field channels and dynamical channels may contribute similar fractions of the observed binary black hole population, whilst Wong et al. (2021) use a mixture of predictions from isolated binary evolution and dynamical formation in globular clusters and find that less than half of the observed binary black holes formed through isolated binary evolution in their models. Bouffanais et al. (2019) and Bouffanais et al. (2021b) find support for contributions from both isolated binary evolution and dynamical formation (in their case, in young star clusters). Safarzadeh (2020), modelling the spin distribution of binary black holes, argue that more than half of the population should arise from dynamical encounters, whereas Tauris (2022) claims that the spin distribution of binary black holes can be explained due to the reorientation of black hole spins at formation. It seems that, despite using a range of different methods and models, the current consensus in the literature is that there are likely contributions from multiple formation channels to the observed binary black hole population.

Another interesting constraint can be obtained directly from Figure 6. We see that approximately 40% of observed binary black holes that can have formed through isolated binary evolution (as discussed above) have chirp masses less than $20 M_{\odot}$. Binary black holes formed through chemically homogeneous evolution are predominantly expected to be formed at low metallicity and have chirp masses greater than $20 M_{\odot}$ (Mandel & de Mink 2016; de Mink & Mandel 2016). Therefore, around 40% of binary black holes have chirp masses which are too low to have formed through the chemically homogeneous evolution channel (see Section 4.2). This

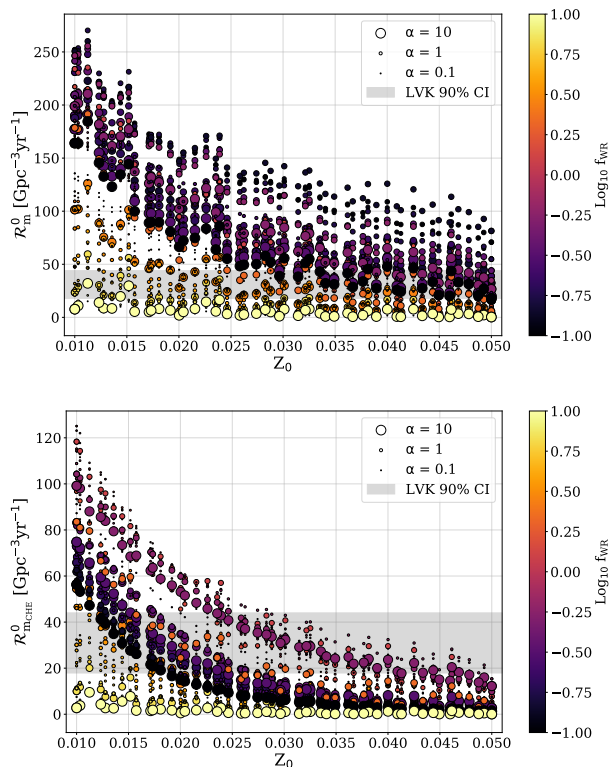


Figure 8. Predicted binary black hole merger rate at redshift $z = 0$ from our models as a function of model hyperparameters. The top panel shows the total predicted binary black hole merger rate from all formation channels, whilst the bottom panel shows only the contribution from the chemically homogeneous evolution channel. The shaded grey region in both panels shows the range of intrinsic binary black hole merger rates inferred by Abbott et al. (2021c).

therefore places a lower limit on the fraction of observed binary black holes formed through other channels. Or alternatively, one can view this as an upper limit of around 60% on the fraction of all detected binary black holes that may have formed through chemically homogeneous evolution. We discuss the uncertainties in the chemically homogeneous evolution channel further in Section 5.

4 MODEL PREDICTIONS

4.1 Binary black hole merger rates

We begin by showing the intrinsic binary black hole merger rate at redshift $z = 0$, as determined from Equation 12, in Figure 8 as a function of our model hyperparameters. We find a large range of merger rates, ranging from $10\text{--}400 \text{ Gpc}^{-3} \text{ yr}^{-1}$. This emphasises just how much variation is possible within these models, given the current level of uncertainties (see also Broekgaard et al. 2022a and Mandel & Broekgaard 2022).

The top panel of Figure 8 shows the total intrinsic binary black hole merger rate at redshift $z = 0$ from all isolated binary evolution pathways modelled within COMPAS. We can identify several trends. We find that models with reduced Wolf–Rayet mass-loss rates tend to predict larger rates than models with higher mass-loss rates. Increased mass-loss during the Wolf–Rayet stage impacts the binary black hole merger rate in a couple of ways. Increased mass-

loss trivially leads to collapsing stars being less massive. This can lead to a larger fraction of binaries being disrupted by the natal kick given to the black holes at birth (particularly for the first born black hole in wide binaries), as lower mass black holes receive larger kicks than high-mass black holes in our model. In addition to this, for tight binaries, the range of orbital periods that allow for chemically homogeneous evolution is narrow (e.g., Mandel & de Mink 2016; Riley et al. 2021), and increased mass-loss can lead to the orbits of these binaries widening enough that the component stars can no longer evolve homogeneously. We show the contribution to the intrinsic binary black hole merger rate from the chemically homogeneous evolution channel only in the bottom panel of Figure 8, as well as in Figure 9. We see that both of the effects described above are much stronger for the population formed through chemically homogeneous evolution. We also see a general trend in Figure 8 that models with larger values of Z_0 typically predict lower binary black hole merger rates, as the increased metallicity also corresponds to higher typical mass-loss rates. This has a similar effect as changing the Wolf–Rayet mass-loss rates, as described above. We do not see any clear trends with the efficiency of common envelope evolution, and this is likely due to the subdominant contribution of this population to the total merger rate in our model. Similarly, we do not see any strong trends with d .

We have also overplotted the binary black hole merger rate inferred by Abbott et al. (2021c) in Figure 8, noting that these rates are inferred using a phenomenological mass distribution fit to the full population of binary black hole mergers. As discussed in the introduction, Abbott et al. (2021c) estimate the intrinsic merger rate of binary black holes to be $\mathcal{R}_{\text{LVK}} = 17\text{--}45 \text{ Gpc}^{-3} \text{ yr}^{-1}$ at a redshift of $z = 0.2^5$. This estimate is sensitive to the overall shape of the binary black hole mass distribution, particularly at low mass, where the intrinsic rate may be high but the observed rate may be low due to selection effects. Abbott et al. (2021c) infer the shape of the binary black hole mass distribution using a series of phenomenological models; our physical models directly predict both the intrinsic binary black hole merger rate and the shape of the mass distribution (as discussed further below). We note that \mathcal{R}_{LVK} is the rate for the whole binary black hole population, integrated over all masses; since a significant fraction ($\sim 10\%$) of observed binary black holes have masses greater than can be produced through isolated binary evolution (see Section 3), we expect that the rate from isolated binary evolution of models matching observations should be less than that found by Abbott et al. (2021c). We discuss the constraints on our models implied by this comparison further in Section 4.3.

We show the fraction of merging binary black holes formed through the chemically homogeneous evolution channel in Figure 9. In the COMPAS fiducial model, around 70% of observable binary black holes are formed through chemically homogeneous evolution (Riley et al. 2021). In our models, we find a large range in the fraction of merging binary black holes formed this way, from less than 20% up to around 70%. Due to the strong gravitational-wave selection effects favouring the higher masses produced through the chemically homogeneous evolution channel (as discussed further in Section 4.2), we find that more than 70% of the observed population is formed through chemically homogeneous evolution in all of our models, and in some models up to 95% of all observed binary black holes are formed through this channel. We find that the largest

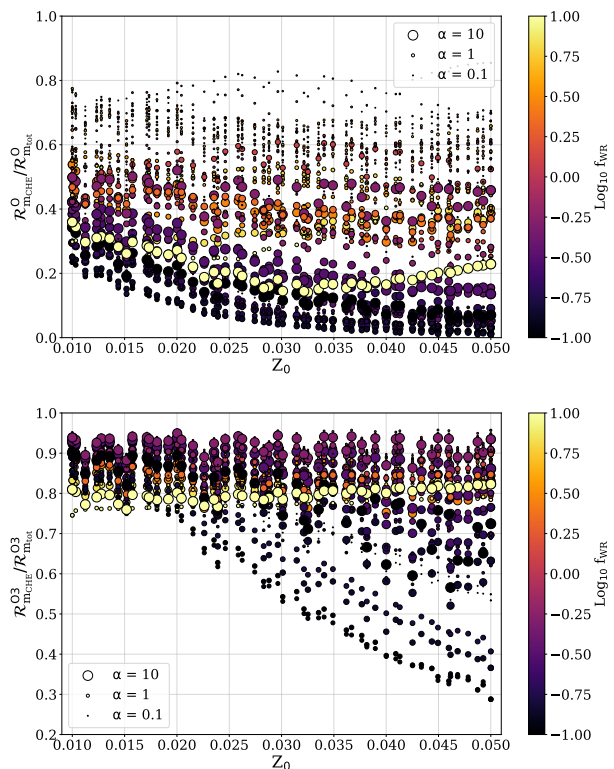


Figure 9. Fraction of merging binary black holes formed through the chemically homogeneous evolution channel, shown as a function of model hyperparameters. The top panel shows the intrinsic fraction, whilst the bottom panel shows the observed fraction accounting for selection effects.

fractions correspond to the models with the smallest values of α_{CE} , as these models have the smallest contribution from the classical common envelope channel (Belczynski et al. 2016b; Stevenson et al. 2017a). We see that smaller fractions of observable binary black holes are formed through chemically homogeneous evolution in models with high values of f_{WR} (bottom panel of Figure 9). This is because the enhanced mass loss causes many tight binaries to widen such that they can no longer merge within the age of the Universe.

The detection rates of binary black hole mergers predicted by our models (as calculated using Equation 14) are shown in Figure 10, again as a function of model hyperparameters. For a single Advanced LIGO detector operating at sensitivity comparable to that achieved during O3, our models predict 10–800 detections per year. Assuming a duration for O3 of $T_{\text{obs}} = 275$ days (Abbott et al. 2021d,b), the actual detection rate was around 100 per year. The exact duration of data analysed varies between analysis pipelines (Abbott et al. 2021d,b). However, we do not expect small changes in our assumed T_{obs} to qualitatively change our results. We summarise the durations of each observing run and the number of detections made in Table 2.

4.2 Binary black hole mass distribution

In addition to impacting the overall rate of binary black hole mergers, we also expect that variations in our assumptions will lead to differences in the mass distribution of binary black holes. Whilst it is difficult to summarise a distribution in a single number, here we opt to use the median observed chirp mass \mathcal{M}_{med} as a summary

⁵ Abbott et al. (2021c) quote the BBH merger rate at $z = 0.2$ as this is close to the redshift where most of the BBHs have been observed, and thus where the rate is best measured (see also Roulet et al. 2020).

Observing run	Catalogues	References	Duration (T_{obs}) [d]	N_{BBH}
O1	GWTC-1	Abbott et al. (2016a, 2019)	48	3
O2	GWTC-1	Abbott et al. (2019)	118	7
O3a	GWTC-2, GWTC-2.1	Abbott et al. (2021d,a)	149 (177)	36
O3b	GWTC-3	Abbott et al. (2021b)	126 (142)	33

Table 2. Summary of the first three observing runs of Advanced LIGO and Virgo. We list the name of each observing run, the name and references for the catalogue(s) from which we draw our observations, along with the duration of each observing run that at least two (one) interferometers were operational. N_{BBH} denotes the number of binary black holes observed during each observing run.

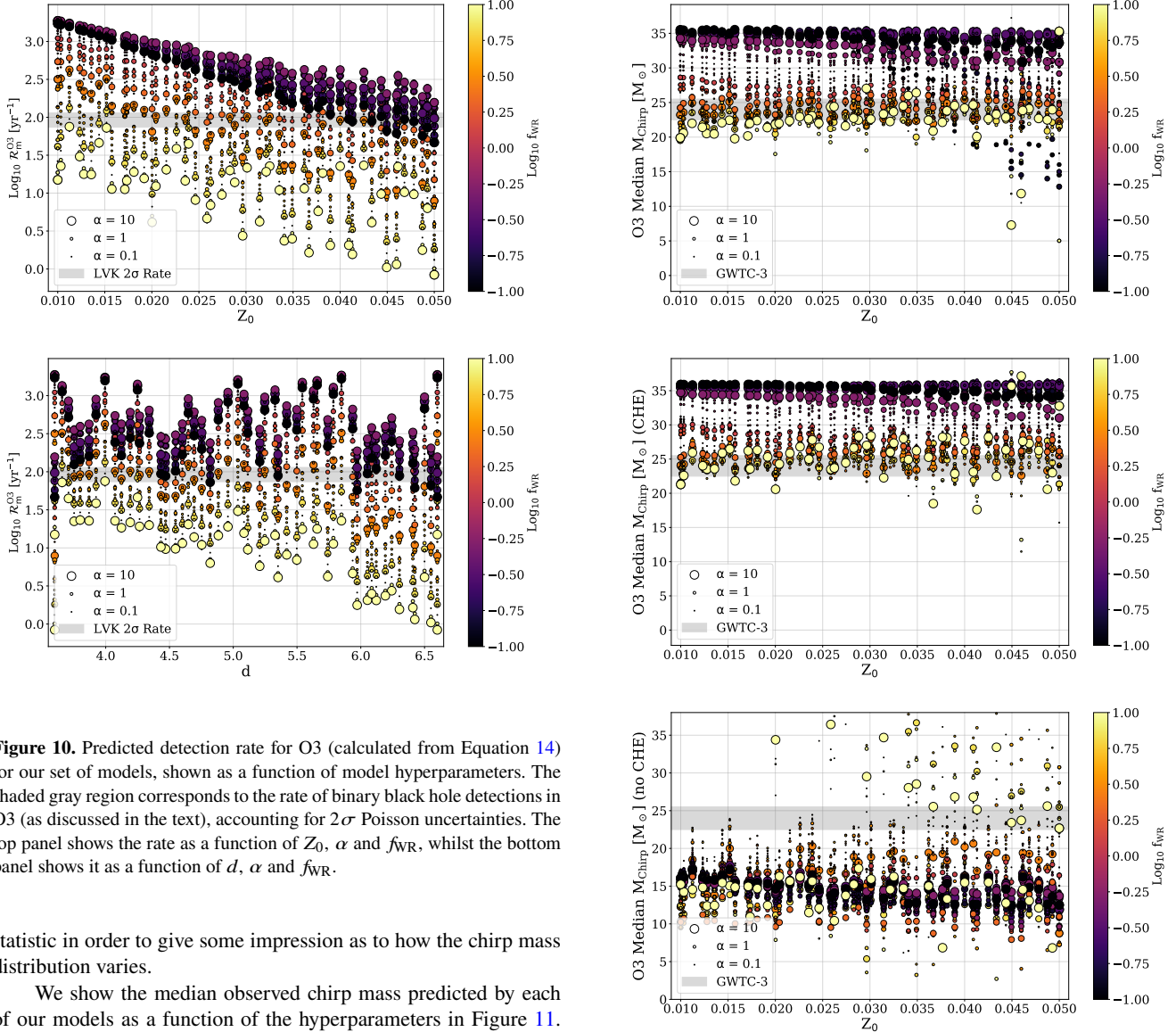


Figure 10. Predicted detection rate for O3 (calculated from Equation 14) for our set of models, shown as a function of model hyperparameters. The shaded gray region corresponds to the rate of binary black hole detections in O3 (as discussed in the text), accounting for 2σ Poisson uncertainties. The top panel shows the rate as a function of Z_0 , α and f_{WR} , whilst the bottom panel shows it as a function of d , α and f_{WR} .

statistic in order to give some impression as to how the chirp mass distribution varies.

We show the median observed chirp mass predicted by each of our models as a function of the hyperparameters in Figure 11. We find that the distribution of chirp masses can vary quite significantly, with variations of more than $10 M_{\odot}$ in predictions for the median chirp mass, ranging anywhere from $22\text{--}34 M_{\odot}$. We find that the median observed chirp mass has a strong dependence on the assumed mass-loss rates for Wolf–Rayet stars (as prescribed by our f_{WR} parameter). In agreement with previous studies ([Riley et al. 2021](#)), we find that binary black holes formed through the chemically homogeneous evolution channel typically have higher average chirp masses ($24\text{--}34 M_{\odot}$; middle panel of Figure 11) compared to other isolated binary evolution formation channels ($10\text{--}23 M_{\odot}$; bottom panel of Figure 11). We find that neither Z_0 nor d have a strong impact on the median observed chirp mass. We also observe from

Figure 11. Median observed chirp mass of binary black holes predicted in our models as a function of the model hyperparameters. The top panel includes all merging binary black holes, whilst the middle panel shows only those formed through chemically homogeneous evolution and the bottom panel shows all formation channels except chemically homogeneous evolution. The shaded grey region indicates the median chirp mass of observed binary black holes ([Abbott et al. 2021b](#)), as described in the text in Section 4.2

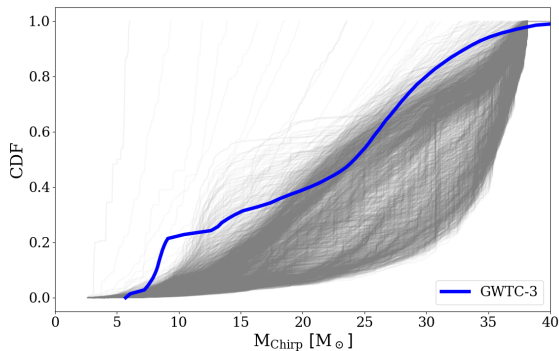


Figure 12. Cumulative observed chirp mass distributions predicted by all of our models are shown in gray, while the empirically determined chirp mass distribution (as shown in Figure 6) is shown in blue. Our models typically predict too many high-mass binary black holes.

the bottom panel of Figure 11 that models with the lowest values of α_{CE} produce binary black holes with higher typical masses; we believe that this is because in these extreme models, most common envelope events result in mergers, and so this population then becomes dominated by the stable mass transfer channel, which typically produces more massive binary black holes than the common envelope channel (Neijssel et al. 2019; Bavera et al. 2021b; van Son et al. 2022b).

In the bottom panel of Figure 6 we estimate the median of the observed chirp mass distribution. We determine that the median observed chirp mass is 24–25 M_{\odot} . We overlay this on Figure 11. Whilst some models are able to reproduce the average observed chirp mass when including binaries formed through chemically homogeneous evolution, most models do not predict enough massive binary black holes when excluding the chemically homogeneous evolution channel (bottom panel of Figure 11). We discuss the constraints implied for our models in Section 4.3.

In our models, we find that binary black holes formed through chemically homogeneous evolution have chirp masses greater than 7 M_{\odot} (Riley et al. 2021). du Buisson et al. (2020) find merging binary black holes formed through chemically homogeneous evolution with chirp masses down to 15 M_{\odot} . This would increase the fraction of the observed binary black holes consistent with forming through chemically homogeneous evolution (quoted in Section 3) to $\sim 70\%$.

We show the chirp mass distributions predicted by our model in Figure 12. There is a large amount of variety in the chirp mass distribution of merging binary black holes predicted by COMPAS. However, we find that even among our broad range of models, none of these models produces a satisfactory match to the observed chirp mass distribution, with almost all models overpredicting the masses of binary black holes (our model distributions are shifted to the right compared to observations). There are a few reasons why this may be the case. Firstly, by construction we have limited the number of uncertain binary evolution assumptions we have explored, and other stages could also have a large impact on both the rate and mass distribution of merging binary black holes (e.g., Broekgaarden et al. 2022a). Secondly, with the exception of the events included in Section 3, we assume that all of the observed merging binary black holes formed through isolated binary evolution. Of course, this may not necessarily be true, and other channels may contribute to the

binary black hole population in the mass range we consider as well. Zevin et al. (2021) fit the observed binary black hole population using models of several different formation channels, and show that a mixture of different formation channels (including both isolated binary evolution and dynamical formation channels) can provide a good match to the overall properties of the observed binary black hole population.

4.3 Comparison to observed rate and chirp mass distribution

Since the focus of the paper is on exploring the predictions of the COMPAS population synthesis model as a function of the uncertain population parameters, a full comparison between the results presented here and the observed gravitational-wave population is deemed beyond the scope of this paper and left for future work (see also discussion in Section 5).

However, it is of course still useful to do some simple comparisons in order to determine if the predictions from these models compare well with observations. We note that previous studies using COMPAS have made comparisons with gravitational-wave observations and found good agreement (e.g., Stevenson et al. 2017a; Neijssel et al. 2019; Riley et al. 2021; Broekgaarden et al. 2022a).

We constrain our models by selecting only those models that simultaneously match both the observed binary black hole rate and the average binary black hole chirp mass, as shown in Figures 10 and 11. Specifically, for the observed binary black hole detection rate, we keep any model that predicts a rate similar to the observed rate in O3, within 2σ (90%) Poisson uncertainties (as indicated by the shaded region in Figure 10). We opt to use the detection rate, rather than the merger rate, as the former is more constraining. For constraining models based on their predicted mass distributions, we make a simple cut, keeping only those models that predict a median chirp mass in the range 22.5–25.5 M_{\odot} , as observed. We show all models that simultaneously match both of these constraints in Figure 13. Out of our 2,916 models, 145 models match the O3 detection rate, 583 models match the median chirp mass only and 79 models match both the median chirp mass and rate.

We find that only models with $f_{\text{WR}} \gtrsim 1$ are capable of explaining both the observed rate of binary black hole mergers, and the mass distribution. This predominantly removes some of the massive binary black holes formed through the CHE channel, both lowering the overall predicted merger rate and reducing the average mass (Figure 9). As can be seen from Figure 13, this is somewhat degenerate with our choice of the typical metallicity of star formation (Z_0), since higher metallicities also lead to higher mass-loss rates (Vink & de Koter 2005). We have quantified the anti-correlation between Z_0 and f_{WR} by calculating both the Spearman and Pearson correlation coefficients, which are -0.719 and -0.745 respectively. Both of these report statistically significant anti-correlations, with p -values $p \ll 0.01$ in both cases.

A similar anti-correlation can be observed in Figure 13 between f_{WR} and d , where large values of d correspond to low star formation rates at high redshift (cf. Figure 3), removing the contribution of low metallicity star formation at high redshift responsible for producing massive binary black holes (predominantly through chemically homogeneous evolution). We again quantified the magnitude of this anti-correlation, finding significant ($p \ll 0.01$) Spearman and Pearson correlation coefficients of -0.438 and -0.514 . These degeneracies are examples of exactly the sorts of correlations that we set out to uncover, and can only be found by exploring the impact of multiple parameters simultaneously.

In Figure 14 we zoom in on the correlation between f_{WR} and

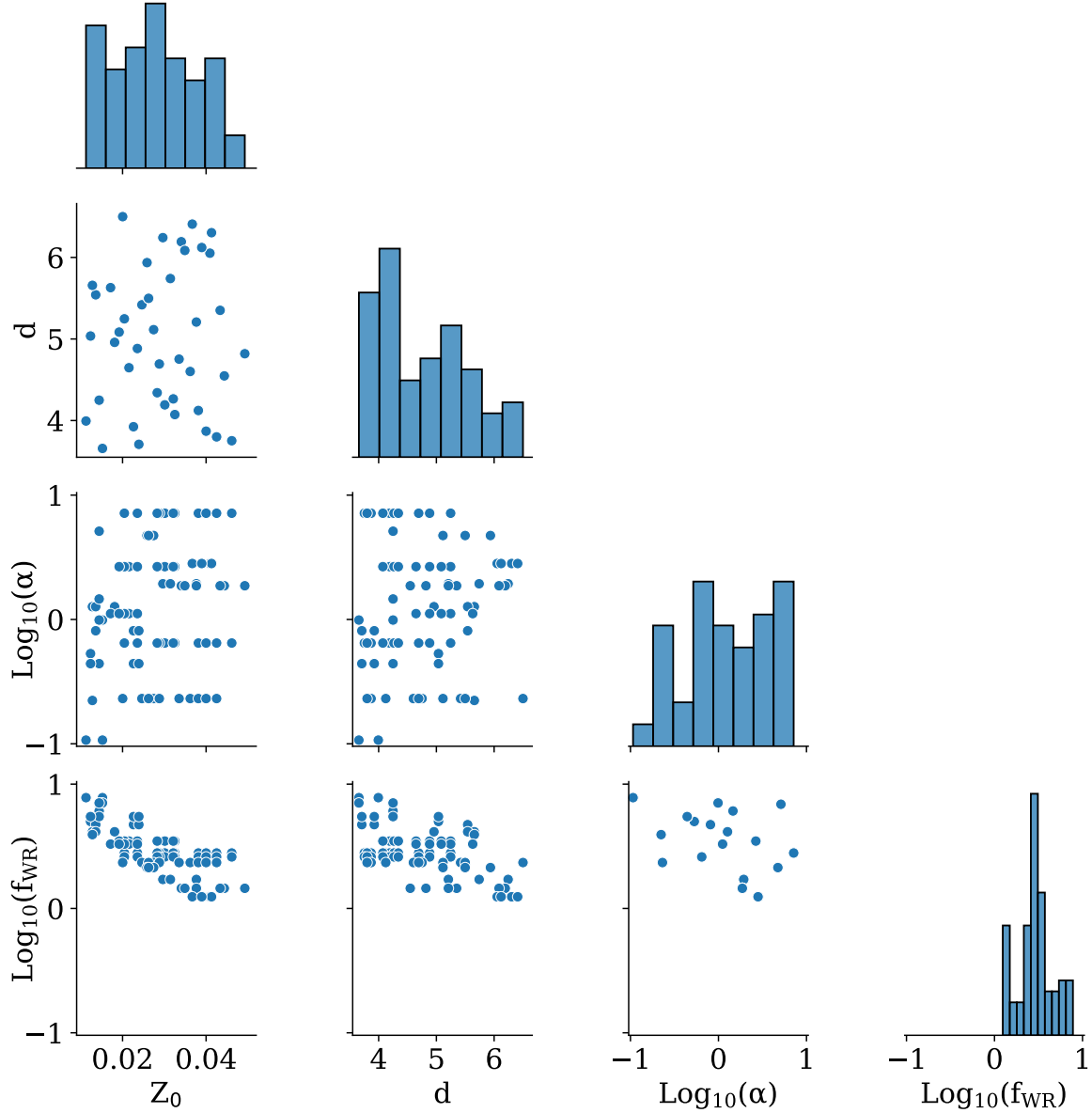


Figure 13. Matrix corner plot showing the one- and two-dimensional distributions of the hyperparameters for which our models match both the observed rate and average mass of binary black holes (for details, see Section 4.3).

Z_0 . We overplot the constraints that $f_{\text{WR}} \lesssim 0.3$ from [Neijssel et al. \(2021\)](#) based upon the mass of the black hole in Cyg X-1 ([Miller-Jones et al. 2021](#)). Our findings are in tension with both these recent observational developments, as well as recent theoretical work on Wolf–Rayet mass loss ([Sander & Vink 2020](#)). As we discuss below, this highlights potential biases that could arise when inferring binary evolution parameters due to limitations of our model (in particular, the modelling of chemically homogeneous evolution).

Most of our models with $\alpha_{\text{CE}} < 1$ are ruled out (see Figure 13). This is because binary black holes formed through the classical common envelope channel typically have the lowest masses out of the

several isolated binary evolution subchannels modelled in COMPAS (see e.g., [van Son et al. 2022b](#)). A population of low-mass binary black holes is required to match the observed mass distribution (Figure 12). Other similar studies have also shown a preference for super-efficient common envelope evolution (e.g., [Santoliquido et al. 2021](#); [Wong et al. 2021](#); [García et al. 2021](#); [Broekgaarden & Berger 2021](#)). [Bouffanais et al. \(2021a\)](#) performed a similar analysis to the one we have performed here. Using similar models of isolated binary evolution, [Bouffanais et al. \(2021a\)](#) vary the efficiency of mass transfer (assuming a single value for all mass transfer episodes with a non-degenerate accretor) and the efficiency of common envelope

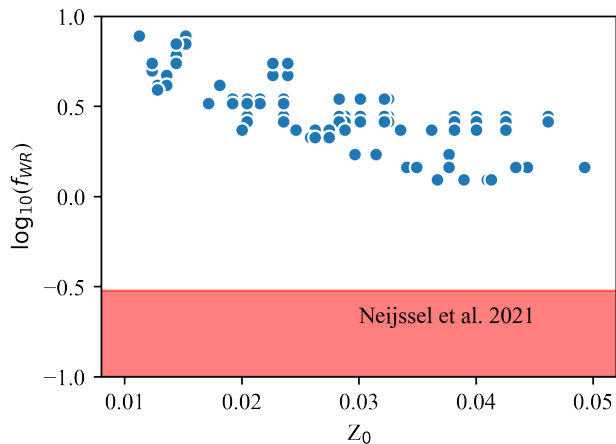


Figure 14. The correlation between the mass-loss rates of Wolf–Rayet stars (f_{WR}) and the typical metallicity of star formation at redshift $z = 0$ (Z_0) for surviving models. The shaded red region shows the observational constraints placed on f_{WR} from the mass of the black hole in Cyg X-1 (Miller-Jones et al. 2021; Neijssel et al. 2021) showing the clear tension with our findings.

evolution. Only considering models with $\alpha_{\text{CE}} > 1$, they find that their preferred models have $\alpha_{\text{CE}} \sim 6$.

Our results are strongly sensitive to the inclusion of the chemically homogeneous evolution channel for forming binary black holes within COMPAS. In Figure 15 we show the fraction of binary black holes formed through chemically homogeneous evolution for the subset of models matching observations (as shown in Figure 13). In models that simultaneously match both the observed binary black hole rate and median chirp mass, 75–90% of binary black holes with chirp masses less than $40 M_{\odot}$ are formed through chemically homogeneous evolution. At present, COMPAS is the only rapid population synthesis that self-consistently includes the chemically homogeneous evolution channel (Riley et al. 2021), though see Ghodla et al. (2022) for details of a recent implementation in the BPASS code (Eldridge et al. 2017). Any constraints on the underlying physics of binary evolution obtained with rapid binary population synthesis codes that do not self consistently include chemically homogeneous evolution may be strongly biased at present.

We now turn to the question of why most of our models predict too many binary black holes with high chirp masses. By default, the implementation of chemically homogeneous evolution in COMPAS (Riley et al. 2021) allows for the stable evolution of binaries in contact at birth, so called massive overcontact binaries (cf. Marchant et al. 2016). However, the physics of contact binaries is not well understood (Abdul-Masih et al. 2022), and these overcontact binaries could be responsible for the discrepancy between our model predictions and observations. As an alternate model, we investigated how our predictions would change if we excluded binaries that are in contact at birth. Figure 16 shows the median chirp mass and the fraction of binary black holes formed through CHE detected in O3 neglecting over-contact binaries. We find that the predictions are similar to when completely excluding all binaries formed through chemically homogeneous evolution, as most of these binaries begin their evolution as over-contact binaries. When excluding over-contact binaries from the population, these models typically underpredict the median binary black hole chirp mass compared to the observed value, as $\lesssim 20\%$ of binary black holes are predicted

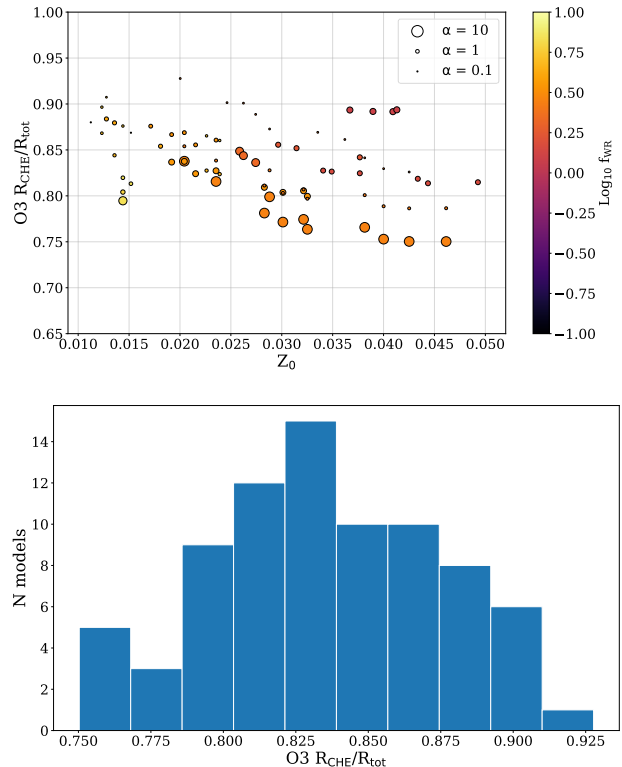


Figure 15. Fraction of merging binary black holes with chirp masses $< 40 M_{\odot}$ formed through the chemically homogeneous evolution channel after constraining our models with observations. The top panel shows the fraction as function of model hyperparameters, while the bottom panel shows a histogram of the fraction for all allowed models.

to be formed through chemically homogeneous evolution due to the small parameter space available avoiding Roche-lobe overflow (Marchant et al. 2016; Riley et al. 2021).

Another element of binary evolution that we have neglected in this paper so far is kicks associated with black hole formation. In our default model used elsewhere in this paper, the kicks of black holes are significantly reduced compared to those of neutron stars through fallback (Fryer et al. 2012), resulting in many of the most massive black holes receiving no kick at formation. Black hole kicks would act to disrupt more binaries, reducing our overall predicted merger rates, and could alter the mass distribution of binary black holes (e.g., Wysocki et al. 2018). We have performed some test simulations to investigate whether allowing for large kicks associated with black hole formation could explain the difference between our models and the observed population. We calculated some test models where we include the impact of large kicks associated with black hole formation, drawn from a Maxwellian distribution and not reducing the kick magnitude due to fallback. Figure 17 shows the results of varying the typical kick magnitude on the chirp mass distribution of the models, keeping all other parameters fixed to the COMPAS defaults (Team COMPAS: Riley et al. 2022). For all models the mass distribution is still peaked at higher masses than the observations, with the lowest kicks (which are close to our default assumptions) being closest to observations. This is likely because our model predictions are dominated by high-mass binary black holes formed through chemically homogeneous evolution, which would require extremely large kicks to be disrupted. We conclude

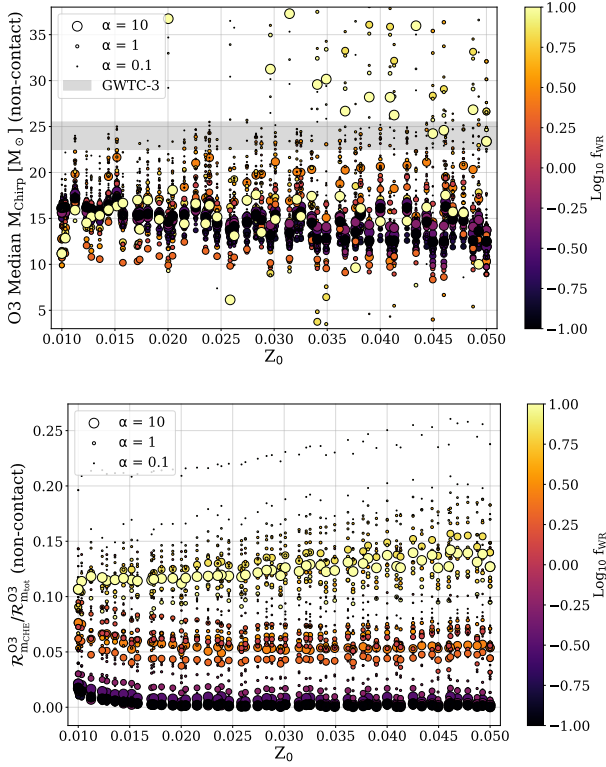


Figure 16. Top: The median chirp mass predicted to be observed in O3 as a function of model hyperparameters, discounting binaries which begin the main sequence in contact. The plot is extremely similar to the distribution when no CHE binaries are included (cf. bottom panel of Figure 11), since the majority of the binaries that undergo CHE in our simulations are actually over-contact binaries. Bottom: The fraction of detected binary black holes formed through the CHE channel when we discount all binaries that start the main sequence as contact binaries. This fraction is decreased dramatically (compared to Figure 9) when we exclude the contact binaries, as the majority of merging binary black holes formed through CHE begin their lives already in contact (cf. Marchant et al. 2016).

that moderate to high black hole kicks cannot explain the discrepancy between our models and observations. Regardless, such high black hole kicks are strongly disfavoured by independent observations (e.g., see discussion in Callister et al. 2021).

5 DISCUSSION AND CONCLUSION

In this paper we have investigated the correlated impact of multiple uncertainties in the evolution of massive binary stars across cosmic time on the population of merging binary black holes observable by current ground-based gravitational-wave observatories.

We made use of the rapid binary population synthesis suite COMPAS (Stevenson et al. 2017a; Vigna-Gómez et al. 2018; Team COMPAS: Riley et al. 2022). We focused on a few specific examples of uncertain evolutionary stages in massive binary evolution. Specifically, we investigated:

- the efficiency of common envelope evolution (α_{CE})
- the mass loss rates of helium-rich Wolf–Rayet stars (f_{WR})
- the cosmic star formation rate at high redshift (d)
- the average gas-phase metallicity of star forming material (Z_0)

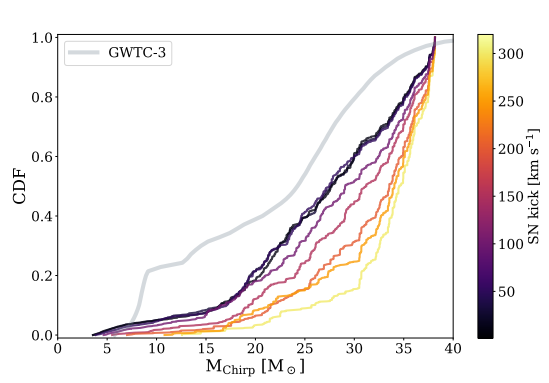


Figure 17. Cumulative density functions of the distribution of binary black hole chirp masses computed for eight populations with different assumptions about the typical supernova kick magnitudes black holes receive at formation. The other population parameters were kept at their default values in COMPAS (Team COMPAS: Riley et al. 2022). For comparison, the empirical mass distribution obtained following GWTC-3 shown in black (Abbott et al. 2021b). While smaller kicks associated with black hole formation shift the distribution towards the observed distribution, none of the kicks tested can produce predictions which satisfactorily match the observations.

We simulated a large number ($N = 2916$) of binary populations, where multiple parameters were allowed to vary from their default values (cf. Figure 1). Our goal was to fully explore the (hyper)parameter space of this population synthesis model, and identify correlations or degeneracies between multiple population hyperparameters. We identified a correlation between the impact of the mass-loss rates for Wolf–Rayet stars (f_{WR}) and the average metallicity of star formation at redshift 0 (Z_0) on the properties of merging binary black holes, as can be seen clearly in Figure 8 and the bottom left panel of Figure 13. This correlation arises as increasing both parameters leads to increase in the amount of mass lost through stellar winds.

Our primary conclusion is that a large amount of variation is possible within models of isolated binary evolution given present uncertainties (cf. Figure 8 and Figure 12). Whilst many of our models can produce binary black hole merger rates in agreement with observations (cf. Figure 8), none of the models we consider provide a good match to the observed binary black hole mass distribution (Figure 12). The models that are closest to the observations require enhanced (high) mass-loss rates for helium rich Wolf–Rayet stars ($f_{WR} > 1$, see Figure 13). This is because high mass-loss rates reduce both the mass of black holes, and the overall binary black hole merger rate, particularly of those formed through chemically homogeneous evolution (Figure 9). Such high mass-loss rates are in tension with recent theoretical and observational developments regarding the winds of Wolf–Rayet stars (e.g., Sander & Vink 2020; Neijssel et al. 2021).

There are a number of possible reasons that our models tend to produce binary black holes that are too massive in comparison to observations. For example, we have restricted our analysis to the four hyperparameters described above, both to limit the computational cost of the model exploration (as discussed in Section 2.6) and to aid in interpreting the results. However, there are a number of additional uncertainties in massive binary evolution which are also important in predictions for binary black holes (Broekgaarden et al. 2022a).

Future work should also expand the analysis presented here to other population hyperparameters, corresponding to other un-

certain stages of massive binary evolution beyond those varied in this study. This could include mass-loss rates during other stages of binary evolution (Barrett et al. 2018), the efficiency and stability of mass transfer (Kruckow et al. 2018; Broekgaarden et al. 2022a; Bouffanais et al. 2021a; Bavera et al. 2021a), and supernova kicks imparted to neutron stars and black holes at birth (e.g., Zevin et al. 2017; Wysocki et al. 2018; Callister et al. 2021; Stevenson 2022). Similarly, other hyperparameters governing the metallicity specific star formation rate (including the particular parameterisation) should be varied in order to fully explore its impact on the population of merging binary black holes (see e.g., Chruślińska 2022; van Son et al. 2022a). As mentioned earlier, some parameters may be more important for some populations than others (cf. Broekgaarden et al. 2022a). Another uncertainty that we have not accounted for in the present analysis concerns the evolution of massive stars. Even detailed stellar models can disagree wildly on the properties of massive stars, which can have a dramatic impact on predictions for the formation of merging binary black holes (Marchant et al. 2021; Klencki et al. 2021; Gallegos-Garcia et al. 2021; Agrawal et al. 2021). Work is underway to allow these uncertainties to be incorporated into rapid population synthesis codes (Kruckow et al. 2018; Spera et al. 2019; Agrawal et al. 2020; Fragos et al. 2022). We leave exploring the impact of these parameters to future work.

We have focused our model exploration primarily on predictions for the mass distribution and merger rate of binary black holes. Another key gravitational-wave observable is the spin of black holes (e.g., Wysocki et al. 2018; Gerosa et al. 2018; Belczynski et al. 2020; Bavera et al. 2020, 2021b; Broekgaarden et al. 2022b). Recent binary evolution models typically predict that the first born black hole is born with negligible spin due to the majority of the stars’ angular momentum being efficiently transported from the stellar core to the envelope (Spruit 2002; Fuller et al. 2019) and then removed through stellar winds and binary mass transfer (Fuller & Ma 2019; Qin et al. 2018). The progenitor of the second born black hole may be tidally spun up if the orbital period of the binary is short enough, leading to some fraction of second born black holes having rapid rotation (Qin et al. 2018; Zaldarriaga et al. 2018; Bavera et al. 2020; Bavera et al. 2021a). Mass ratio reversal occurring through mass transfer may allow for the more massive black hole to be born second in some fraction of binary black holes, allowing for the possibility of them to be rapidly rotating (Zevin & Bavera 2022; Broekgaarden et al. 2022b). Binary black holes formed through chemically homogeneous evolution may have large aligned spins (Marchant et al. 2016). It is likely that some of the hyperparameters we have varied here, such as the mass-loss rates of Wolf–Rayet stars, will have an observable impact on the spin distribution of observable binary black holes.

Our population synthesis model assumes a universal efficiency for the common envelope phase of massive binary evolution. The common envelope efficiency parameter may not be universal, and may for example depend on the properties of the binary (such as the mass ratio) at the time the common envelope phase occurs (De Marco et al. 2011; Davis et al. 2012). Since binary black holes may form from progenitors with similar properties (in terms of significant mass ratios and wide orbits) it may be that this approximation is not too bad in this case. However, it is likely that, even if gravitational-wave observations do provide a precise measurement of α_{CE} , that should be considered as only applying to massive binary black hole progenitors, and a different value of α_{CE} may be applicable for other populations (for example, Zorotovic et al. 2010, find that $\alpha_{\text{CE}} \sim 0.2\text{--}0.3$ provides a good match to a sample of low-mass post common envelope binaries consisting of white dwarfs and

main sequence stars). Furthermore, the energy formalism (Webbink 1984) may not be the correct description of the common envelope for massive stars (e.g., Nelemans et al. 2000). We argue that even in this case, our results may still be interpretable. For example, some of our more extreme models (with $\alpha_{\text{CE}} \ll 1$) result in a dramatic reduction in the formation rate of binary black holes through common envelope evolution as many binaries that would otherwise form that way end up merging during the common envelope phase (cf. Figure 9). These models may therefore still be relevant if binary black hole formation through common envelope evolution is rare, even if that rarity is due to another reason, as discussed by Klencki et al. (2021) and Marchant et al. (2021).

In this paper we focused on binary black holes as these have the largest number of observations to compare against so far. Recent studies have shown that different populations of double compact objects are sensitive to different binary evolution physics (Broekgaarden et al. 2021; Broekgaarden et al. 2022a). For example, Broekgaarden et al. (2022a) find that predictions for binary neutron stars are not sensitive to uncertainties in the cosmic star formation history, since in these models, the formation of neutron star binaries is much less sensitive to metallicity than black hole formation. Similar results have been found by others including Tang et al. (2020). In the future, we will need to expand our analysis to include both binary neutron star and neutron star-black hole binaries. We note that previous work has shown that predictions from COMPAS are broadly in agreement with the observed rates and properties of binary neutron star and neutron star-black hole binaries for a range of model choices (Vigna-Gómez et al. 2018; Chattopadhyay et al. 2020; Chattopadhyay et al. 2021; Broekgaarden et al. 2022a; Broekgaarden & Berger 2021; Broekgaarden et al. 2021; Chattopadhyay et al. 2022).

Several observed gravitational-wave events have properties that are difficult to explain through isolated binary evolution (e.g., GW190521 and GW190814), though several groups of authors have proposed counterarguments (Zevin et al. 2020; Antoniadis et al. 2022; Costa et al. 2020; Belczynski 2020). We have assumed that any binary black hole with a chirp mass greater than $40 M_{\odot}$ cannot be formed through isolated binary evolution, consistent with our models (though see Costa et al. 2020; Belczynski 2020; Liu & Bromm 2020; Kinugawa et al. 2021, for counter arguments). Under this assumption, we argue that at least 10% of observed binary black hole mergers must have a formation channel other than classical isolated binary evolution of massive, metal poor population I/II stars (Figure 7). Leading candidates include dynamical formation in dense stellar environments such as young star clusters (Di Carlo et al. 2020a), old globular clusters (Rodríguez et al. 2018) or the discs around active galactic nuclei (Yang et al. 2019). We similarly argued that the 40% of binary black holes with chirp masses less than $20 M_{\odot}$ cannot have formed through chemically homogeneous evolution (Mandel & de Mink 2016; de Mink & Mandel 2016), placing an upper limit of around 50% on the fraction of detected binary black holes that can have formed through that channel. These inferences qualitatively agree with the findings of Zevin et al. (2021) (see their Figure 4) who used a mixture model consisting of population synthesis model predictions for several different formation scenarios to constrain the fraction of binary black holes formed through each channel. Whilst our approach is somewhat different, we find this overall agreement reassuring.

Regardless of the specific subchannel, we have assumed that all binary black holes with chirp masses less than $40 M_{\odot}$ are formed through isolated binary evolution. However, it is of course possible (and even likely) that there are additional contributions from

these other channels, though determining the formation channel for any given event is extremely difficult. Attempting to constrain binary evolution parameters whilst including events formed through other channels will inevitably lead to biases in the estimates of the population parameters (and thus of our understanding of binary evolution). One approach that can be employed to mitigate this issue is to combine models of multiple formation scenarios, and include the branching ratios between these scenarios as an additional parameter to be fit (e.g., Zevin et al. 2017, 2021; Stevenson et al. 2017b; Wong et al. 2021; Bouffanais et al. 2019; Bouffanais et al. 2021b). Another way to mitigate these biases is to complement modelled analyses with model independent analyses that search for subpopulations of gravitational-wave sources with similar properties (Mandel et al. 2017; Powell et al. 2019). Another possibility is to infer the population hyperparameters that best reproduce each individual event; if extreme assumptions are required to explain a particular event, it again might indicate a different formation scenario (Wong et al. 2022).

This work is intended to form the first stage of our analysis of gravitational-wave observations. One of our eventual goals is to be able to constrain these parameters (and thus massive binary evolution) by comparing our models to observations (Barrett et al. 2018). Even though population synthesis codes such as COMPAS are extremely fast, capable of simulating a population of 10^6 binaries in ~ 12 hrs, it is still infeasible to directly use COMPAS to fully explore the parameter space, where potentially millions (or even more) of likelihood evaluations would be required. One can think of our exploration here as a coarse, manual exploration of a restricted parameter space, rather than an automated exploration using a stochastic sampling technique such as Markov-Chain Monte Carlo or Nested Sampling (Skilling 2006). There are several approaches one could take in order to fully explore the (hyper)parameter space with these approaches. One option could be to construct an emulator which can interpolate the predictions of a limited set of population synthesis models. Some early work exploring interpolation of population synthesis models was made by Barrett et al. (2016) and Taylor & Gerosa (2018). This approach typically utilises methods such as machine learning (e.g., deep flow, random forest regression or neural networks) or Gaussian process regression (Barrett et al. 2016; Taylor & Gerosa 2018; Lin et al. 2021; Wong & Gerosa 2019; Wong et al. 2021). These approximate, emulated models are then fast enough to evaluate to be used in a likelihood evaluation in a stochastic sampler, whilst also allowing for the model to be evaluated at any arbitrary set of hyperparameters. Another option (which is less explored in this context) would be to perform inference with a sparse set of models, and then interpolate the likelihood (e.g., Smith et al. 2014; Abbott et al. 2016b).

As with all population models, detailed binary evolution models of chemically homogeneous evolution have several important uncertainties. One of the primary sources of uncertainty is the mass-loss rates, as already discussed in Section 2.3. In addition to the mass-loss rates of helium rich stars, the mass-loss rates of hydrogen rich, chemically homogeneously evolving main-sequence stars are likely underestimated in COMPAS, as the fits in COMPAS assume that these stars have the same luminosity as a ‘normal’ main-sequence star of the same mass and age (Riley et al. 2021). However, a chemically homogeneously evolving star is expected to be more luminous than a conventionally evolving star of the same mass, which would lead to increased mass-loss rates on the main-sequence. This could potentially cause some binaries to widen sufficiently to exit the parameter space for chemically homogeneous evolution. Beyond the uncertainties in the mass-loss rates, the main uncertainty in mod-

els of chemically homogeneous evolution involves the treatment of rotationally enhanced mixing in one-dimensional stellar evolution codes, and the range of masses, rotation rates and orbital periods that allow for chemically homogeneous evolution (see Mandel & de Mink 2016, for deeper discussion). Chemically homogeneous evolution is predominantly a theoretical phenomena at present, although a handful of observations over recent years have highlighted systems which can potentially (only) be explained through this channel (Martins et al. 2013; Almeida et al. 2015; Abdul-Masih et al. 2021). Attempts to constrain the chemically homogeneous evolution pathway through observations of stars are difficult due to the strong preference for low metallicity environments. Whilst we found a preference for models with high Wolf–Rayet mass-loss rates (and correspondingly lower binary black hole merger rates), an alternative interpretation could be that our model allows too many binaries to undergo chemically homogeneous evolution, and alternative, more stringent models should be considered.

ACKNOWLEDGEMENTS

We thank Ilya Mandel, Alejandro Vigna-Gómez and Tom Callister for useful comments and discussions. We thank the referee for a careful reading of the manuscript. The authors are supported by the Australian Research Council (ARC) Centre of Excellence for Gravitational Wave Discovery (OzGrav), through project number CE170100004. SS is supported by the ARC Discovery Early Career Research Award DE220100241. T. A. C. receives support from the Australian Government Research Training Program. This work was performed on the OzSTAR national facility at Swinburne University of Technology. The OzSTAR program receives funding in part from the Astronomy National Collaborative Research Infrastructure Strategy (NCRIS) allocation provided by the Australian Government.

DATA AVAILABILITY

This work made use of the publicly available binary population synthesis suite COMPAS (Team COMPAS: Riley et al. 2022). COMPAS is available at <https://github.com/TeamCOMPAS/COMPAS>. Results produced for this paper are available upon request.

REFERENCES

- Aasi J., et al., 2015, *Class. Quant. Grav.*, 32, 074001
- Abbott B. P., et al., 2016a, *Phys. Rev. X*, 6, 041015
- Abbott B. P., et al., 2016b, *Phys. Rev. D*, 94, 064035
- Abbott B. P., et al., 2017, *Phys. Rev. Lett.*, 119, 161101
- Abbott B. P., et al., 2019, *Phys. Rev.*, X9, 031040
- Abbott B. P., et al., 2020a, *Living Reviews in Relativity*, 23, 3
- Abbott R., et al., 2020b, *Phys. Rev. Lett.*, 125, 101102
- Abbott B. P., et al., 2020c, *Astrophys. J. Lett.*, 892, L3
- Abbott R., et al., 2020d, *Astrophys. J. Lett.*, 896, L44
- Abbott R., et al., 2020e, *Astrophys. J. Lett.*, 900, L13
- Abbott R., et al., 2021a, arXiv e-prints, p. arXiv:2108.01045
- Abbott R., Abbott T. D., Acernese F., Ackley K., Adams C., Adhikari N., Adhikari R. X., et al., 2021b, arXiv e-prints, p. arXiv:2111.03606
- Abbott R., Abbott T. D., Acernese F., Ackley K., Adams C., Adhikari N., Adhikari R. X., et al. 2021c, arXiv e-prints, p. arXiv:2111.03634
- Abbott R., et al., 2021d, *Physical Review X*, 11, 021053
- Abbott R., et al., 2021e, *Astrophys. J. Lett.*, 913, L7
- Abbott R., et al., 2021f, *Astrophys. J. Lett.*, 915, L5

- Abdul-Masih M., et al., 2021, *A&A*, **651**, A96
- Abdul-Masih M., Escorza A., Menon A., Mahy L., Marchant P., 2022, arXiv e-prints, p. [arXiv:2208.01671](https://arxiv.org/abs/2208.01671)
- Acernese F., et al., 2015, *Class. Quant. Grav.*, **32**, 024001
- Agrawal P., Hurley J., Stevenson S., Szécsi D., Flynn C., 2020, *MNRAS*, **497**, 4549
- Agrawal P., Szécsi D., Stevenson S., Hurley J., 2021, arXiv e-prints, p. [arXiv:2112.02800](https://arxiv.org/abs/2112.02800)
- Almeida L. A., et al., 2015, *ApJ*, **812**, 102
- Antoniadis J., et al., 2022, *Astron. Astrophys.*, **657**, L6
- Astropy Collaboration et al., 2013, *A&A*, **558**, A33
- Astropy Collaboration et al., 2018, *AJ*, **156**, 123
- Astropy Collaboration et al., 2022, arXiv e-prints, p. [arXiv:2206.14220](https://arxiv.org/abs/2206.14220)
- Banerjee S., Kroupa P., Oh S., 2012, *MNRAS*, **426**, 1416
- Barlow M. J., Smith L. J., Willis A. J., 1981, *MNRAS*, **196**, 101
- Barrett J. W., Mandel I., Neijssel C. J., Stevenson S., Vigna-Gomez A., 2016, *IAU Symp.*, **325**, 46
- Barrett J. W., Gaebel S. M., Neijssel C. J., Vigna-Gómez A., Stevenson S., Berry C. P. L., Farr W. M., Mandel I., 2018, *Mon. Not. Roy. Astron. Soc.*, **477**, 4685
- Bavera S. S., et al., 2020, *Astron. Astrophys.*, **635**, A97
- Bavera S. S., Zevin M., Fragos T., 2021a, *Research Notes of the American Astronomical Society*, **5**, 127
- Bavera S. S., et al., 2021b, *Astron. Astrophys.*, **647**, A153
- Beasar E. R., Davies B., Smith N., van Loon J. T., Gehrz R. D., Figer D. F., 2020, *MNRAS*, **492**, 5994
- Belczynski K., 2020, *Astrophys. J. Lett.*, **905**, L15
- Belczynski K., Kalogera V., Rasio F. A., Taam R. E., Bulik T., 2007, *Astrophys. J.*, **662**, 504
- Belczynski K., Bulik T., Fryer C. L., Ruiter A., Valsecchi F., Vink J. S., Hurley J. R., 2010, *ApJ*, **714**, 1217
- Belczynski K., Holz D. E., Bulik T., O’Shaughnessy R., 2016a, *Nature*, **534**, 512
- Belczynski K., et al., 2016b, *Astron. Astrophys.*, **594**, A97
- Belczynski K., et al., 2020, *Astron. Astrophys.*, **636**, A104
- Belczynski K., et al., 2022, *ApJ*, **925**, 69
- Bestenlehner J. M., et al., 2011, *A&A*, **530**, L14
- Boco L., Lapi A., Chruslinska M., Donevski D., Sicilia A., Danese L., 2021, *Astrophys. J.*, **907**, 110
- Bouffanais Y., Mapelli M., Gerosa D., Di Carlo U. N., Giacobbo N., Berti E., Baibhav V., 2019, *ApJ*, **886**, 25
- Bouffanais Y., Mapelli M., Santoliquido F., Giacobbo N., Iorio G., Costa G., 2021a, *Mon. Not. Roy. Astron. Soc.*, **505**, 3873
- Bouffanais Y., Mapelli M., Santoliquido F., Giacobbo N., Di Carlo U. N., Rastello S., Artale M. C., Iorio G., 2021b, *Mon. Not. Roy. Astron. Soc.*, **507**, 5224
- Breivik K., et al., 2020, *Astrophys. J.*, **898**, 71
- Briel M. M., Eldridge J. J., Stanway E. R., Stevance H. F., Chrimes A. A., 2022, *Mon. Not. Roy. Astron. Soc.*, **514**, 1315
- Broekgaarden F. S., Berger E., 2021, *Astrophys. J. Lett.*, **920**, L13
- Broekgaarden F. S., et al., 2019, *Mon. Not. Roy. Astron. Soc.*, **490**, 5228
- Broekgaarden F. S., et al., 2021, *Mon. Not. Roy. Astron. Soc.*, **508**, 5028
- Broekgaarden F. S., et al., 2022a, *MNRAS*,
- Broekgaarden F. S., Stevenson S., Thrane E., 2022b, arXiv e-prints, p. [arXiv:2205.01693](https://arxiv.org/abs/2205.01693)
- Bustillo J. C., Sanchis-Gual N., Torres-Forné A., Font J. A., 2021, *Phys. Rev. Lett.*, **126**, 201101
- Callister T. A., Farr W. M., Renzo M., 2021, *Astrophys. J.*, **920**, 157
- Chattopadhyay D., Stevenson S., Hurley J. R., Rossi L. J., Flynn C., 2020, *Mon. Not. Roy. Astron. Soc.*, **494**, 1587
- Chattopadhyay D., Stevenson S., Hurley J. R., Bailes M., Broekgaarden F., 2021, *MNRAS*, **504**, 3682
- Chattopadhyay D., Stevenson S., Broekgaarden F., Antonini F., Belczynski K., 2022, *MNRAS*, **513**, 5780
- Chruslinska M., 2022, arXiv e-prints, p. [arXiv:2206.10622](https://arxiv.org/abs/2206.10622)
- Chruslinska M., Nelemans G., 2019, *MNRAS*, **488**, 5300
- Chruslinska M., Nelemans G., Belczynski K., 2019, *Mon. Not. Roy. Astron. Soc.*, **482**, 5012
- Costa G., Bressan A., Mapelli M., Marigo P., Iorio G., Spera M., 2020, *MNRAS*,
- Crowther P. A., Schnurr O., Hirschi R., Yusof N., Parker R. J., Goodwin S. P., Kassim H. A., 2010, *MNRAS*, **408**, 731
- Davis P. J., Kolb U., Knigge C., 2012, *MNRAS*, **419**, 287
- De Marco O., Passy J.-C., Moe M., Herwig F., Mac Low M.-M., Paxton B., 2011, *MNRAS*, **411**, 2277
- Di Carlo U. N., Mapelli M., Bouffanais Y., Giacobbo N., Santoliquido F., Bressan A., Spera M., Haardt F., 2020a, *Mon. Not. Roy. Astron. Soc.*, **497**, 1043
- Di Carlo U. N., et al., 2020b, *Mon. Not. Roy. Astron. Soc.*, **498**, 495
- Dominik M., Belczynski K., Fryer C., Holz D., Berti E., Bulik T., Mandel I., O’Shaughnessy R., 2012, *Astrophys. J.*, **759**, 52
- Dominik M., et al., 2015, *Astrophys. J.*, **806**, 263
- Eldridge J. J., Stanway E. R., Xiao L., McClelland L. A. S., Taylor G., Ng M., Greis S. M. L., Bray J. C., 2017, *Publ. Astron. Soc. Australia*, **34**, e058
- Enia A., et al., 2022, arXiv e-prints, p. [arXiv:2202.00019](https://arxiv.org/abs/2202.00019)
- Farmer R., Renzo M., de Mink S. E., Marchant P., Justham S., 2019, *ApJ*, **887**, 53
- Farr W. M., Stevenson S., Coleman Miller M., Mandel I., Farr B., Vecchio A., 2017, *Nature*, **548**, 426
- Farrell E. J., Groh J. H., Hirschi R., Murphy L., Kaiser E., Ekström S., Georgy C., Meynet G., 2021, *Mon. Not. Roy. Astron. Soc.*, **502**, L40
- Figer D. F., 2005, *Nature*, **434**, 192
- Finkelstein S. L., 2016, *Publ. Astron. Soc. Australia*, **33**, e037
- Fragos T., Andrews J. J., Ramirez-Ruiz E., Meynet G., Kalogera V., Taam R. E., Zezas A., 2019, *Astrophys. J. Lett.*, **883**, L45
- Fragos T., et al., 2022, arXiv e-prints, p. [arXiv:2202.05892](https://arxiv.org/abs/2202.05892)
- Fryer C. L., Belczynski K., Wiktorowicz G., Dominik M., Kalogera V., Holz D. E., 2012, *ApJ*, **749**, 91
- Fuller J., Ma L., 2019, *Astrophys. J. Lett.*, **881**, L1
- Fuller J., Piro A. L., Jermyn A. S., 2019, *MNRAS*, **485**, 3661
- Galauge S., Talbot C., Nagar T., Jain D., Thrane E., Mandel I., 2021, *Astrophys. J. Lett.*, **921**, L15
- Gallegos-García M., Berry C. P. L., Marchant P., Kalogera V., 2021, *Astrophys. J.*, **922**, 110
- Gallegos-García M., Fishbach M., Kalogera V., Berry C. P. L., Doctor Z., 2022, arXiv e-prints, p. [arXiv:2207.14290](https://arxiv.org/abs/2207.14290)
- García F., Bunzel A. S., Chaty S., Porter E., Chassande-Mottin E., 2021, *Astron. Astrophys.*, **649**, A114
- Gayathri V., et al., 2022, *Nature Astronomy*
- Gerosa D., Berti E., O’Shaughnessy R., Belczynski K., Kesden M., Wysocki D., Gladysz W., 2018, *Phys. Rev. D*, **98**, 084036
- Ghodla S., Eldridge J. J., Stanway E. R., Stevance H. F., 2022, preprint
- Giacobbo N., Mapelli M., Spera M., 2018, *Mon. Not. Roy. Astron. Soc.*, **474**, 2959
- Grichener A., Soker N., 2021, *Mon. Not. Roy. Astron. Soc.*, **507**, 1651
- Hamann W. R., Koesterke L., 1998, *A&A*, **335**, 1003
- Hamann W. R., et al., 2019, *A&A*, **625**, A57
- Higgins E. R., Sander A. A. C., Vink J. S., Hirschi R., 2021, *Mon. Not. Roy. Astron. Soc.*, **505**, 4874
- Hinshaw G., et al., 2013, *ApJS*, **208**, 19
- Hurley J. R., Pols O. R., Tout C. A., 2000, *MNRAS*, **315**, 543
- Hurley J. R., Tout C. A., Pols O. R., 2002, *MNRAS*, **329**, 897
- Iaconi R., De Marco O., 2019, *MNRAS*, **490**, 2550
- Ivanova N., 2018, *Astrophys. J. Lett.*, **858**, L24
- Ivanova N., et al., 2013, *A&ARv*, **21**, 59
- Ivanova N., Justham S., Podsiadlowski P., 2015, *Mon. Not. Roy. Astron. Soc.*, **447**, 2181
- Kewley L., Kobulnicky H. A., 2005, in de Grijs R., González Delgado R. M., eds, *Astrophysics and Space Science Library Vol. 329, Starbursts: From 30 Doradus to Lyman Break Galaxies*. p. 307, doi:10.1007/1-4020-3539-X_55
- Khan S., Husa S., Hannam M., Ohme F., Pürrer M., Forteza X. J., Bohé A., 2016, *Phys. Rev. D*, **93**, 044007
- Kinugawa T., Nakamura T., Nakano H., 2021, *Mon. Not. Roy. Astron. Soc.*, **501**, L49

- Klencki J., Moe M., Gladysz W., Chruslinska M., Holz D. E., Belczynski K., 2018, *Astron. Astrophys.*, 619, A77
- Klencki J., Nelemans G., Istrate A. G., Chruslinska M., 2021, *Astron. Astrophys.*, 645, A54
- Kroupa P., 2001, *Mon. Not. Roy. Astron. Soc.*, 322, 231
- Kruckow M. U., Tauris T. M., Langer N., Szécsi D., Marchant P., Podsiadlowski P., 2016, *A&A*, 596, A58
- Kruckow M. U., Tauris T. M., Langer N., Kramer M., Izzard R. G., 2018, *Mon. Not. Roy. Astron. Soc.*, 481, 1908
- Lamberts A., et al., 2018, *MNRAS*, 480, 2704
- Langer N., Norman C. A., 2006, *Astrophys. J. Lett.*, 638, L63
- Lau M. Y. M., Hirai R., González-Bolívar M., Price D. J., De Marco O., Mandel I., 2022, *Mon. Not. Roy. Astron. Soc.*, 512, 5462
- Law-Smith J. A. P., et al., 2020, arXiv eprint
- Lin L., Bingham D., Broekgaarden F., Mandel I., 2021, arXiv eprint
- Liu B., Bromm V., 2020, *Astrophys. J. Lett.*, 903, L40
- Madau P., Dickinson M., 2014, *Ann. Rev. Astron. Astrophys.*, 52, 415
- Madau P., Fragos T., 2017, *Astrophys. J.*, 840, 39
- Maeder A., 1987, *A&A*, 178, 159
- Mandel I., Broekgaarden F. S., 2022, *Living Reviews in Relativity*, 25, 1
- Mandel I., Farmer A., 2022, *Phys. Rept.*, 955, 1
- Mandel I., de Mink S. E., 2016, *Mon. Not. Roy. Astron. Soc.*, 458, 2634
- Mandel I., Farr W. M., Colonna A., Stevenson S., Tiño P., Veitch J., 2017, *Mon. Not. Roy. Astron. Soc.*, 465, 3254
- Mandel I., Müller B., Riley J., de Mink S. E., Vigna-Gómez A., Chattopadhyay D., 2020, *Mon. Not. Roy. Astron. Soc.*, 500, 1380
- Mapelli M., Giacobbo N., 2018, *Mon. Not. Roy. Astron. Soc.*, 479, 4391
- Mapelli M., Giacobbo N., Ripamonti E., Spera M., 2017, *Mon. Not. Roy. Astron. Soc.*, 472, 2422
- Mapelli M., Santoliquido F., Bouffanais Y., Sedda M. A., Artale M. C., Ballone A., 2021a, *Symmetry*, 13, 1678
- Mapelli M., et al., 2021b, *Mon. Not. Roy. Astron. Soc.*, 505, 339
- Marchant P., Langer N., Podsiadlowski P., Tauris T. M., Moriya T. J., 2016, *Astron. Astrophys.*, 588, A50
- Marchant P., Renzo M., Farmer R., Pappas K. M. W., Taam R. E., de Mink S. E., Kalogera V., 2019, *ApJ*, 882, 36
- Marchant P., Pappas K. M. W., Gallegos-García M., Berry C. P. L., Taam R. E., Kalogera V., Podsiadlowski P., 2021, *Astron. Astrophys.*, 650, A107
- Martins F., Depagne E., Russeil D., Mahy L., 2013, *A&A*, 554, A23
- Mauron N., Josselin E., 2011, *A&A*, 526, A156
- McKay M. D., Beckman R. J., Conover W. J., 1979, *Technometrics*, 21, 239
- Miller-Jones J. C. A., et al., 2021, *Science*, 371, 1046
- Moe M., Di Stefano R., 2017, *ApJS*, 230, 15
- Moreno M. M., Schneider F. R. N., Roepke F. K., Ohlmann S. T., Pakmor R., Podsiadlowski P., Sand C., 2021, *A&A*
- Morris M. D., Mitchell T. J., 1995, *Journal of Statistical Planning and Inference*, 43, 381
- Neijssel C. J., et al., 2019, *MNRAS*, 490, 3740
- Neijssel C. J., Vinciguerra S., Vigna-Gomez A., Hirai R., Miller-Jones J. C. A., Bahramian A., Maccarone T. J., Mandel I., 2021, *Astrophys. J.*, 908, 118
- Nelemans G., Verbunt F., Yungelson L. R., Portegies Zwart S. F., 2000, *A&A*, 360, 1011
- Ng K. K. Y., Vitale S., Zimmerman A., Chatziioannou K., Gerosa D., Haster C.-J., 2018, *Phys. Rev. D*, 98, 083007
- Nitz A. H., Kumar S., Wang Y.-F., Kastha S., Wu S., Schäfer M., Dhurkunde R., Capano C. D., 2021, arXiv eprint
- Nugis T., Lamers H. J. G. L. M., 2000, *A&A*, 360, 227
- O'Shaughnessy R., Bellovary J. M., Brooks A., Shen S., Governato F., Christensen C. R., 2017, *MNRAS*, 464, 2831
- Olsen S., Venumadhav T., Mushkin J., Roulet J., Zackay B., Zaldarriaga M., 2022, arXiv eprint
- Paczynski B., 1967, *Acta Astron.*, 17, 355
- Paczynski B., 1976, in Eggleton P., Mitton S., Whelan J., eds, Vol. 73, *Structure and Evolution of Close Binary Systems*. p. 75
- Paxton B., Bildsten L., Dotter A., Herwig F., Lesaffre P., Timmes F., 2011, *ApJS*, 192, 3
- Peters P. C., 1964, *Physical Review*, 136, 1224
- Pols O. R., Schröder K.-P., Hurley J. R., Tout C. A., Eggleton P. P., 1998, *MNRAS*, 298, 525
- Powell J., Stevenson S., Mandel I., Tino P., 2019, *Mon. Not. Roy. Astron. Soc.*, 488, 3810
- Qin Y., Fragos T., Meynet G., Andrews J., Sørensen M., Song H. F., 2018, *Astron. Astrophys.*, 616, A28
- Qin Y., Marchant P., Fragos T., Meynet G., Kalogera V., 2019, *Astrophys. J. Lett.*, 870, L18
- Reichardt T. A., De Marco O., Iaconi R., Chamandy L., Price D. J., 2020, *MNRAS*, 494, 5333
- Renzo M., Ott C. D., Shore S. N., de Mink S. E., 2017, *A&A*, 603, A118
- Renzo M., Cantiello M., Metzger B., Jiang Y.-F., 2020, *Astrophys. J. Lett.*, 904, L13
- Riley J., Mandel I., Marchant P., Butler E., Nathaniel K., Neijssel C., Short S., Vigna-Gomez A., 2021, *Mon. Not. Roy. Astron. Soc.*, 505, 663
- Rodriguez C. L., Chatterjee S., Rasio F. A., 2016, *Phys. Rev. D*, 93, 084029
- Rodriguez C. L., Amaro-Seoane P., Chatterjee S., Rasio F. A., 2018, *Phys. Rev. Lett.*, 120, 151101
- Romero-Shaw I. M., Lasky P. D., Thrane E., Bustillo J. C., 2020, *Astrophys. J. Lett.*, 903, L5
- Romero-Shaw I. M., Lasky P. D., Thrane E., 2021, *Astrophys. J. Lett.*, 921, L31
- Romero-Shaw I. M., Lasky P. D., Thrane E., 2022, arXiv eprint
- Roulet J., Venumadhav T., Zackay B., Dai L., Zaldarriaga M., 2020, *Phys. Rev. D*, 102, 123022
- Safarzadeh M., 2020, *Astrophys. J. Lett.*, 892, L8
- Sana H., et al., 2012, *Science*, 337, 444
- Sander A. A. C., Vink J. S., 2020, *MNRAS*, 499, 873
- Santoliquido F., Mapelli M., Giacobbo N., Bouffanais Y., Artale M. C., 2021, *Mon. Not. Roy. Astron. Soc.*, 502, 4877
- Skilling J., 2006, *Bayesian Analysis*, 1, 833
- Smith N., 2017, *Philosophical Transactions of the Royal Society of London Series A*, 375, 20160268
- Smith R. J. E., Hanna C., Mandel I., Vecchio A., 2014, *Phys. Rev. D*, 90, 044074
- Soker N., Grichener A., Gilkis A., 2019, *Mon. Not. Roy. Astron. Soc.*, 484, 4972
- Spera M., Mapelli M., Giacobbo N., Trani A. A., Bressan A., Costa G., 2019, *MNRAS*, 485, 889
- Spruit H. C., 2002, *Astron. Astrophys.*, 381, 923
- Stevenson S., 2022, *Astrophys. J. Lett.*, 926, L32
- Stevenson S., Ohme F., Fairhurst S., 2015, *Astrophys. J.*, 810, 58
- Stevenson S., Vigna-Gómez A., Mandel I., Barrett J. W., Neijssel C. J., Perkins D., de Mink S. E., 2017a, *Nature Communications*, 8, 14906
- Stevenson S., Berry C. P. L., Mandel I., 2017b, *Mon. Not. Roy. Astron. Soc.*, 471, 2801
- Stevenson S., Sampson M., Powell J., Vigna-Gómez A., Neijssel C. J., Szécsi D., Mandel I., 2019, *ApJ*, 882, 121
- Strolger L.-G., et al., 2004, *ApJ*, 613, 200
- Tang P. N., Eldridge J. J., Stanway E. R., Bray J. C., 2020, *Mon. Not. Roy. Astron. Soc.*, 493, L6
- Tauris T., 2022, arXiv e-prints, p. arXiv:2205.02541
- Tauris T. M., Dewi J. D. M., 2001, *Astron. Astrophys.*, 369, 170
- Taylor S. R., Gerosa D., 2018, *Phys. Rev. D*, 98, 083017
- Team COMPAS: Riley J., et al., 2022, *Astrophys. J. Supp.*, 258, 34
- Tramper F., Sana H., de Koter A., 2016, *ApJ*, 833, 133
- Valsecchi F., Glebbeek E., Farr W. M., Fragos T., Willems B., Orosz J. A., Liu J., Kalogera V., 2010, *Nature*, 468, 77
- Vigna-Gómez A., et al., 2018, *MNRAS*, 481, 4009
- Vink J. S., 2017, *A&A*, 607, L8
- Vink J. S., 2021, arXiv e-prints, p. arXiv:2109.08164
- Vink J. S., de Koter A., 2002, *A&A*, 393, 543
- Vink J. S., de Koter A., 2005, *Astron. Astrophys.*, 442, 587
- Vink J. S., de Koter A., Lamers H. J. G. L. M., 2001, *Astron. Astrophys.*, 369, 574
- Vink J. S., Higgins E. R., Sander A. A. C., Sabhahit G. N., 2021, *Mon. Not. Roy. Astron. Soc.*, 504, 146

- Voss R., Tauris T. M., 2003, *Mon. Not. Roy. Astron. Soc.*, 342, 1169
- Webbink R. F., 1984, *ApJ*, 277, 355
- Wong K. W. K., Gerosa D., 2019, *Phys. Rev. D*, 100, 083015
- Wong K. W. K., Breivik K., Kremer K., Callister T., 2021, *Phys. Rev. D*, 103, 083021
- Wong K. W. K., Breivik K., Farr W. M., Luger R., 2022, arXiv e-prints, p. [arXiv:2206.04062](https://arxiv.org/abs/2206.04062)
- Woosley S., 2017, *Astrophys. J.*, 836, 244
- Wysocki D., Gerosa D., O’Shaughnessy R., Belczynski K., Gladysz W., Berti E., Kesden M., Holz D. E., 2018, *Phys. Rev. D*, 97, 043014
- Xu X.-J., Li X.-D., 2010, *ApJ*, 716, 114
- Yang Y., et al., 2019, *Phys. Rev. Lett.*, 123, 181101
- Yang Y., Bartos I., Haiman Z., Kocsis B., Márka S., Tagawa H., 2020, *Astrophys. J.*, 896, 138
- Yoon S.-C., 2017, *Mon. Not. Roy. Astron. Soc.*, 470, 3970
- Yuan T. T., Kewley L. J., Richard J., 2013, *ApJ*, 763, 9
- Zaldarriaga M., Kushnir D., Kollmeier J. A., 2018, *MNRAS*, 473, 4174
- Zevin M., Bavera S. S., 2022, *Astrophys. J.*, 933, 86
- Zevin M., Pankow C., Rodriguez C. L., Sampson L., Chase E., Kalogera V., Rasio F. A., 2017, *Astrophys. J.*, 846, 82
- Zevin M., Spera M., Berry C. P. L., Kalogera V., 2020, *Astrophys. J. Lett.*, 899, L1
- Zevin M., et al., 2021, *Astrophys. J.*, 910, 152
- Zorotovic M., Schreiber M. R., Gänsicke B. T., Nebot Gómez-Morán A., 2010, *A&A*, 520, A86
- de Kool M., 1990, *ApJ*, 358, 189
- de Mink S. E., Belczynski K., 2015, *Astrophys. J.*, 814, 58
- de Mink S. E., Mandel I., 2016, *Mon. Not. Roy. Astron. Soc.*, 460, 3545
- du Buisson L., et al., 2020, *Mon. Not. Roy. Astron. Soc.*, 499, 5941
- van Son L. A. C., de Mink S. E., Chruslinska M., Conroy C., Pakmor R., Hernquist L., 2022a, preprint
- van Son L. A. C., et al., 2022b, *Astrophys. J.*, 931, 17

This paper has been typeset from a $\text{\TeX}/\text{\LaTeX}$ file prepared by the author.